

Characterization of Cooperators in Quorum Sensing with 2D Molecular Signal Analysis

Yuting Fang, Adam Noel, Andrew W. Eckford, Nan Yang, and Jing Guo

Abstract

In quorum sensing (QS), bacteria exchange molecular signals to work together. An analytically-tractable model is presented for characterizing QS signal propagation within a population of bacteria and the number of responsive cooperative bacteria (i.e., cooperators) in a two-dimensional (2D) environment. Unlike prior works with a deterministic topology and a simplified molecular propagation channel, this work considers continuous emission, diffusion, degradation, and reception among randomly-distributed bacteria. Using stochastic geometry, the 2D channel response and the corresponding probability of cooperation at a bacterium are derived. Based on this probability, new expressions are derived for the moment generating function and different orders of moments of the number of cooperators. The analytical results agree with the simulation results obtained by a particle-based method. In addition, the Poisson and Gaussian distributions are compared to approximate the distribution of the number of cooperators and the Poisson distribution provides the best overall approximation. The derived channel response can be generally applied to any molecular communication model where single or multiple transmitters continuously release molecules into a 2D environment. The derived statistics of the number of cooperators can be used to predict and control the QS process, e.g., predicting and decreasing the likelihood of biofilm formation.

Index Terms

Quorum sensing, molecular communication, 2D channel response, cooperative bacteria

I. INTRODUCTION

Quorum sensing (QS) is a ubiquitous approach for microbial communities to respond to a variety of situations in which monitoring the local population density is beneficial. When bacteria use QS, they assess the number of other bacteria they can interact with by releasing and recapturing a molecular signal in their environment. This is due to the fact that a higher density of bacteria leads to more molecules that can be detected before they diffuse away or become degraded. If the number of molecules detected exceeds a threshold, then bacteria express target genes for a cooperative response. QS enables coordination within large groups of cells, potentially increasing the efficiency of processes that require a large population of cells working together. Microscopic populations utilize QS to

complete many collaborative activities, such as virulence, bioluminescence, biofilms, and the production of antibiotics. These tasks play a crucial role in bacterial infections, environmental remediation, and wastewater treatment [2]. Since the QS process is highly dependent on signaling molecules, an accurate characterization of release, diffusion, degradation, and reception of such molecules across the environment in which bacteria live is very important to understand and control QS, which can help us to prevent undesirable bacterial infections and lead to new environmental remediation methods [3].

There are growing research efforts to study the coordination of bacteria via QS. Among them, [3]–[5] investigated the cooperative behavior of bacteria using simulation or biological experiments and [6]–[11] mathematically modeled bacterial behavior coordination. We note that [6]–[11] relied on abstract or simplifying models to represent the molecular diffusion channel (e.g., they did not consider the motion of individual signaling molecules based on Fick’s laws) in order to focus on understanding how behavior evolves over time. [12] considered a molecular diffusion channel between two clusters of bacteria, but did not consider the bacteria behavioral response. To the best of our knowledge, analyzing the statistics of the number of cooperative bacteria, taking into account the chemical reaction and diffusion of each molecule based on reaction-diffusion dynamics, is not available in the literature.

To control cooperative bacterial activities (e.g., biofilm formation and bioluminescence) for medical treatment and environmental monitoring, an analytically-tractable model needs to be developed since it predicts the cooperative behavior of bacteria, considering their noisy molecular signal propagation. We achieve this goal in this paper by leveraging the knowledge of QS, mass diffusion, stochastic geometry, and probability processes. Since our model accounts for the random motion of molecules based on reaction-diffusion equations, our model can be used to predict and control the impact of environment parameters, e.g., diffusion coefficient, reaction rate, and population density, on the concentration of molecules observed by bacteria and the statistics of the number of responsive cooperative bacteria.

In this paper, we consider a two-dimensional (2D) environment over which the bacteria are randomly spatially distributed according to a point process model. This is motivated by that bacteria may move in realistic environments and their locations may be not fixed. In the point process model, the locations of bacteria are changing between realizations [13], [14]. This means that the number of cooperative bacteria can change from one realization to the next. As a result, we are interested in the average result or distribution of the number of cooperative bacteria over a large number of realizations. We consider a 2D environment since a 2D environment facilitates future experimental validation of our current theoretical work. Biological experiments, especially with bacteria, are usually conducted in a 2D environment, e.g., bacteria residing on a petri dish (i.e., a thin plate for cell-culture) and the

formation of biofilms [15]. While considering the topological randomness of bacteria, our model captures the basic features of QS by adopting the assumptions as follows: We assume that each bacterium acts as both a point transmitter (TX) and a circular receiver (RX), which captures the features of emission and reception of QS molecules. Since bacteria emit molecules sporadically in reality, we assume that each bacterium continuously¹ emits molecules at random times.

We emphasize that developing the analytical model in this paper is theoretically challenging since we need to address the *random* received signal at bacteria in *random* locations due to *randomness* in the motion and degradation of molecules, and *randomness* in the locations of many TXs. Despite these challenges, we make the following theoretical contributions:

- 1) We analytically derive the channel response (i.e., the expected number of molecules observed) at a RX due to continuous emission or an impulse emission of molecules at one point TX. Based on this, we then derive the channel response at a RX due to continuous emission of molecules from point TXs randomly distributed over a circle in a 2D environment.
- 2) Using the results in 1), we first derive the exact expression for the expected probability of cooperation at the bacterium at a fixed location, due to the emission of molecules from randomly-distributed bacteria, by using the Laplace transform of the random aggregate of received molecules. We then derive an approximate expression for such a probability, which is easier to compute than the exact expression, yet from our numerical results has good accuracy when the population density is sufficiently high.
- 3) Based on the results in 2), we derive approximate expressions for the moment generating function (MGF) and cumulant generating function (CGF) of the number of cooperative bacteria (i.e., cooperators). Using the MGF and the CGF, we derive approximate expressions for the n th moment and cumulant of the number of cooperators. We study the convergence of the number of cooperators to a Gaussian distribution via the higher order statistics. We use the Poisson and Gaussian distributions with the derived statistics to analytically fit the probability mass function (PMF) and cumulative distribution function (CDF) of the number of cooperators. We show that the Poisson distribution provides the best overall approximation, based on our numerical results. In addition, we derive the expected number of pairs of two nearest bacteria both cooperating, which can be used to predict clusters of cooperators in a QS system.

We validate the accuracy of our analytical results via a particle-based simulation method where we track the random walk of each signaling molecule over time. In contrast to our preliminary work

¹Note that continuous emission does not mean there is no time interval between two successive emissions of molecules.

in [1], which only derives a portion of the results in 1) and the expected number of cooperators, this paper conducts a more comprehensive analysis of the 2D channel response, derives an exact expression for the expected probability of cooperation, and studies the distribution of the number of cooperators by its MGF and different order statistics.

Our derived statistical moments can help predict and control the QS process. For example, biofilm formation via QS is a mechanism for bacteria to resist antibiotics. However, a biofilm could be prevented from forming if the density of cooperators is too small. Our expressions reveal the impact of environmental factors (e.g., degradation and diffusion rates) on the likelihood of a given number of bacteria choosing to cooperate. Based on our expressions, we could infer how to decrease the likelihood of successful biofilm formation by adjusting environmental parameters. This could help optimize the performance of antibiotic treatment.

While contributing to QS, our results could also be applied to other molecular communication (MC) systems. More specifically, the 2D channel response could be used to determine the expected molecular signal observed at an RX when a TX (or TXs) impulsively or continuously releases molecules into a 2D environment in an MC system. The cooperating probability and statistical moments of the number of cooperators can be applied to study the group behavior of an MC system that uses consensus algorithms and broadcast channel models. For example, a cluster of nanomachines in a nanonetwork could secrete and sense molecules to achieve global network synchronization as proposed in [16]. Our derived cooperating probability and the number of cooperators could be used to determine the probability of a nanomachine being synchronized and the percentage of synchronized nanomachines in the nanonetwork.

We use the following notations: $|\vec{x}|$ denotes Euclidean norm of a vector \vec{x} . \overline{N} denotes the mean of a random variable (RV) N and $\mathbb{E}_{\Phi}\{\cdot\}$ denotes the expectation over a spatial random point process Φ . $K_n(\cdot)$ denotes modified n th order Bessel function of the second kind. $I_n(\cdot)$ denotes the modified n th order Bessel function of the first kind [17]. $\Gamma(a, z)$ denotes the incomplete gamma function.

II. SYSTEM MODEL

We consider an *unbounded* 2D environment. Unlike a deterministic topology model, we consider a point process model to represent topological randomness of bacteria. There are several types of point processes and we consider the Poisson point process (PPP) in this paper [18] due to its tractable properties and well-known theorems. A population of bacteria is spatially distributed over a *bounded* circle S_1 with radius R_1 centered at $(0, 0)$ according to a 2D PPP with constant density λ , as shown in Fig. 1. We denote \vec{x}_i as the location of the center of the bacterium i where the bacterium i is

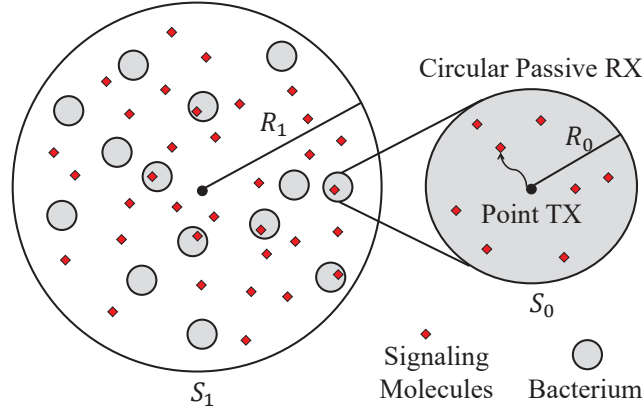


Fig. 1. A population of bacteria randomly distributed over a circle S_1 according to a 2D spatial point process, where each bacterium acts as a point TX and as a circular passive RX S_0 . The molecules diffuse into and out of the bacteria.

an arbitrary bacterium in the bacterial population. We denote $\Phi(\lambda)$ as the set of random bacteria locations. We consider bacteria behavior analogous to QS, i.e., 1) emit signaling molecules; 2) detect the concentration of signaling molecules; and 3) decide to cooperate if the concentration exceeds a threshold. In the following, we detail the emission, propagation, and reception of signaling molecules, and the decision-making by the bacteria.

Emission: We consider that bacterium i continuously releases molecules at different times, as shown in Fig. 2. The release time instants constitute points in a one-dimensional (1D) PPP and one molecule is released at each release time instant. We assume that the continuous emission of each bacterium follows an independent PPP with a rate q . The rate q is the average number of release time events within a unit time (i.e., 1 second). The rate q is also equal to the number of molecules being released per second since one molecule is released at each release time event. We note that [19] and [20] also model molecules being emitted continuously at random times according to a 1D PPP.

Propagation: All A molecules diffuse independently with a constant diffusion coefficient D and they can degrade into a form that cannot be detected by the bacteria, i.e., $A \xrightarrow{k} \emptyset$, where k is the reaction rate constant in s^{-1} . If $k = 0$, this degradation is negligible. Since we consider a single type of molecule, we only mention “the molecules”, i.e., omitting “ A ”, in the remainder of this paper.

Reception: We model the bacterium i as a circular passive RX with radius R_0 and area S_0 centered at \vec{x}_i . The bacterium i samples the number of molecules within S_0 at only **only one time instant** t . Bacteria perfectly count molecules if they are within S_0 . Since the molecules released from all bacteria may be observed by the bacterium i , the number of molecules observed at the bacterium i at time t , $N_{\text{agg}}^\dagger(\vec{x}_i, t|\lambda)$, is given by $N_{\text{agg}}^\dagger(\vec{x}_i, t|\lambda) = \sum_{\vec{x}_j \in \Phi(\lambda)} N(\vec{x}_i, t|\vec{x}_j)$, where $N(\vec{x}_i, t|\vec{x}_j)$ is

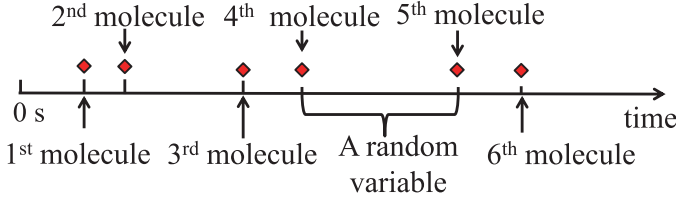


Fig. 2. An example of release times due to continuous emission of molecules at a bacterium according to a random process.

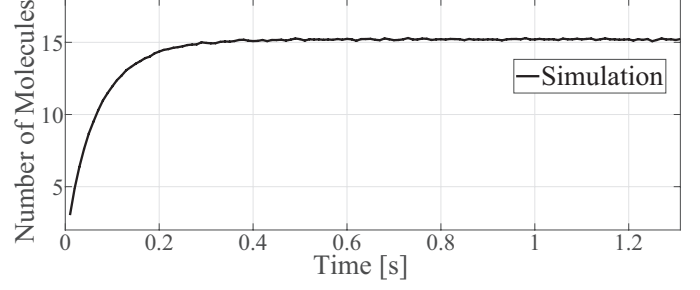


Fig. 3. The average number of molecules observed at time t , $\bar{N}_{\text{agg}}^{\dagger}(\vec{x}_i, t|\lambda)$, versus time t . $R_1 = 20 \mu\text{m}$, $\lambda = 7.9 \times 10^{-2}/\mu\text{m}^2$, $\vec{x}_i = (10 \mu\text{m}, 10 \mu\text{m})$; see other simulation details in Sec. VI.

the number of molecules observed at time t at the bacterium i due to the bacterium j . The means of $N_{\text{agg}}^{\dagger}(\vec{x}_i, t|\lambda)$ and $N(\vec{x}_i, t|\vec{x}_j)$ are denoted by $\bar{N}_{\text{agg}}^{\dagger}(\vec{x}_i, t|\lambda)$ and $\bar{N}(\vec{x}_i, t|\vec{x}_j)$, respectively. We assume that the *expected* number of molecules observed at the bacterium i is constant after some time when degradation occurs. To demonstrate the suitability of this assumption, see Fig. 3 (and an analytical proof in Remark 1). In Fig. 3, $\bar{N}_{\text{agg}}^{\dagger}(\vec{x}_i, t|\lambda)$ is independent of t after time $t \approx 0.5$ s. We denote time t_i^* as the time after which $\bar{N}_{\text{agg}}^{\dagger}(\vec{x}_i, t|\lambda)$ is approximately constant, i.e.,

$$\bar{N}_{\text{agg}}^{\dagger}(\vec{x}_i, t|\lambda)|_{t > t_i^*} \approx \lim_{t \rightarrow \infty} \bar{N}_{\text{agg}}^{\dagger}(\vec{x}_i, t|\lambda) = \bar{N}_{\text{agg}}^{\dagger}(\vec{x}_i, \infty|\lambda). \quad (1)$$

We also refer to any observation after t_i^* , i.e., $\bar{N}_{\text{agg}}^{\dagger}(\vec{x}_i, \infty|\lambda)$, as an asymptotic observation. Notably, similar steady observations at the asymptotic stage have also been shown in [19] and [20].

Decision-Making: We assume that the bacterium i uses its asymptotic observation to make a decision, when the expected number of observed molecules becomes stable. This assumption is reasonable since t_i^* is very small, e.g., $t = 0.5$ s in Fig. 3, and bacteria can reach the steady state very quickly, especially relative to the timescale of gene regulation to coordinate behavior². Also, bacteria can wait until there are enough molecules to trigger behavior change. Therefore, bacteria do not need to explicitly know whether the steady state has been reached and precise synchronization over the population for emission and detection is not needed. Inspired by QS, we consider a threshold-based strategy at bacteria to decide cooperation. We note that the threshold-based strategy is commonly adopted in molecular communication (MC) literature, e.g., [24], [25]. We consider that bacteria compare $N_{\text{agg}}^{\dagger}(\vec{x}_i, \infty|\lambda)$ with a threshold η . If $N_{\text{agg}}^{\dagger}(\vec{x}_i, \infty|\lambda) \geq \eta$, then the bacterium i decides to be a cooperator, otherwise the bacterium i is noncooperative.

²Based on [21]–[23], the cooperation of bacteria is observed after the signaling molecules diffuse for at least tens of minutes.

In the following, we acknowledge the major simplifying assumptions to clarify the applicability of our work and identify areas for future study. These assumptions are as follows:

- 1) We assume that the bacteria do not move over time after being randomly placed in each realization of the 2D PPP. This assumption is reasonable for three reasons: i) There are some non-motile bacteria, e.g., coliform and streptococci; ii) When bacteria swim very slowly, the mobile case can be well approximated by the non-mobile case; and iii) In fact, bacteria often keep stationary when cooperating, e.g., when forming a stable biofilm.
- 2) We consider an ideal transceiver model for bacteria. We simplify bacteria as point sources emitting molecules isotropically into the environment. Considering imperfect TXs is left for future work. We assume that bacteria are passive observers that do not interact with signaling molecules. This is because the observations at multiple bacteria are *correlated* for reactive RXs, which makes analysis much more cumbersome.
- 3) We assume that the average molecule emission rate is constant. We acknowledge that in a real QS process, bacteria may increase their emission rate when they change from being selfish to being cooperative. This assumption is appropriate for scenarios where bacteria transition from being selfish to ramping up molecule production before the emission rate is updated.
- 4) Each bacterium makes one decision based on one sample of the observed signal. We acknowledge that bacteria usually make decisions to cooperate multiple times in their life. Modeling evolutionary or repeat behavior coordination over time with noisy signal propagation is interesting for future work, e.g., as we propose in [26].

III. 2D CHANNEL RESPONSE

In this section, we aim to derive the channel response, i.e., the expected number of molecules observed at a RX, due to continuous emission of molecules from randomly-distributed TXs. To this end, we first derive the channel response due to a point TX as an intermediate step. We assume that the RX is a circular passive observer S_0 centered at \vec{b} with radius R_0 throughout this section, unless specified otherwise. These analyses lay the foundations for our derivations of the observations at bacteria and expected density of cooperators in Sec. IV.

A. One Point TX

In this subsection, we only consider a single TX-RX pair and the point TX is at the point (0,0) for the convenience of analysis. The scenario considered here for this preliminary analysis is distinct from our general system model where multiple TXs exist. We also include the special case when the

TX is at the center of the RX, since each bacterium receives the molecules released not only from other bacteria but also from itself.

Based on [19, eq. (9)], the asymptotic channel response due to *continuous* emission is obtained by multiplying the impulse channel response by the emission rate q and then integrating over all time to infinity. Using this method, the asymptotic channel response is given in the following proposition:

Proposition 1: The asymptotic channel response $\bar{N}(\vec{b}, \infty)$ at \vec{b} , due to continuous emission with rate q from the point $(0, 0)$ since time $t = 0$, is given by

$$\bar{N}(\vec{b}, \infty) = q \int_{\tau=0}^{\infty} \bar{N}_{\text{im}}(\vec{b}, \tau) d\tau, \quad (2)$$

where $\bar{N}_{\text{im}}(\vec{b}, \tau)$ is the channel response at \vec{b} at time τ due to an impulse emission of one molecule at time $t = 0$ from the point $(0, 0)$.

Proof: See Appendix A. ■

Based on Proposition 1, we first derive $\bar{N}_{\text{im}}(\vec{b}, \tau)$ for any \vec{b} and $\vec{b} = 0$ to evaluate $\bar{N}(\vec{b}, \infty)$. We note that the results of $\bar{N}_{\text{im}}(\vec{b}, \tau)$ also can be used in any contexts where a TX emits molecules impulsively. The impulsive emission is commonly considered in the MC literature, which assumed that the TX is a nanomachine having the ability to control the timing of its molecule releases.

1) *Impulse Emission:* We first solve $\bar{N}_{\text{im}}(\vec{b}, \tau)$ for any \vec{b} and then solve the special case when the TX is at the center of the circular RX S_0 , i.e., $|\vec{b}| = 0$. We denote $\bar{N}_{\text{im,self}}(\tau)$ as the channel response at $\vec{b} = (0, 0)$ at time τ due to an impulse emission of one molecule at time $t = 0$ from the point $(0, 0)$, i.e., $\bar{N}_{\text{im,self}}(\tau) = \lim_{\vec{b} \rightarrow 0} \bar{N}_{\text{im}}(\vec{b}, \tau)$. We solve $\bar{N}_{\text{im}}(\vec{b}, \tau)$ for any \vec{b} and $\bar{N}_{\text{im,self}}(\tau)$ in the following theorems.

Theorem 1 (Impulse Emission for Any \vec{b}): The channel response $\bar{N}_{\text{im}}(\vec{b}, \tau)$ for a circular passive observer S_0 centered at any \vec{b} with radius R_0 is given by

$$\begin{aligned} \bar{N}_{\text{im}}(\vec{b}, \tau) = \sum_{i=1}^4 \left\{ \alpha_i \exp\left(-\frac{R_0^2 + |\vec{b}|^2}{4D\tau} - k\tau\right) \left[\exp\left(\frac{R_0^2}{4D\tau}\right) - \exp\left(\frac{R_0|\vec{b}|\beta_i}{2D\tau}\right) \right] \right. \\ \left. + \frac{\alpha_i |\vec{b}|\beta_i \sqrt{D\pi}}{2D\sqrt{\tau}} \exp\left(-\frac{|\vec{b}|^2(1-\beta_i^2)}{4D\tau} - k\tau\right) \left[\text{erf}\left(\frac{|\vec{b}|\beta_i}{2\sqrt{D\tau}}\right) + \text{erf}\left(\frac{R_0 - |\vec{b}|\beta_i}{2\sqrt{D\tau}}\right) \right] \right\}, \quad (3) \end{aligned}$$

where the exact values of α_i and β_i for different ranges of z are given in [27]. Due to the limitation of space, we do not present these exact values here.

Theorem 2 (Impulse Emission for $|\vec{b}| = 0$): The channel response due to an impulse emission from itself is given by

$$\bar{N}_{\text{im,self}}(\tau) = \exp(-k\tau) \left(1 - \exp\left(\frac{-R_0^2}{4D\tau}\right) \right). \quad (4)$$

Proof: The proofs of Theorem 1 and Theorem 2 are given in Appendix B. ■

2) *Continuous Emission*: We then evaluate the asymptotic channel response due to continuous emission for any \vec{b} and $\vec{b} = 0$ in the following theorems.

Theorem 3 (Continuous Emission for Any \vec{b}): The asymptotic channel response $\bar{N}(\vec{b}, \infty)$ for the circular passive RX S_0 centered at any \vec{b} , due to continuous emission with rate q from the point $(0, 0)$ since time $t = 0$, using uniform concentration assumption (UCA) [28], is given by

$$\bar{N}(\vec{b}, \infty) \approx \frac{qR_0^2}{2D} K_0 \left(|\vec{b}| \sqrt{\frac{k}{D}} \right). \quad (5)$$

Theorem 4 (Continuous Emission for $|\vec{b}| = 0$): The asymptotic channel response at the circular RX S_0 , due to continuous emission with rate q from the center of this RX since time $t = 0$, $\bar{N}_{\text{self}}(\vec{b}, \infty)$, is given by

$$\bar{N}_{\text{self}}(\infty) = \frac{q}{k} \left(1 - \frac{\sqrt{k}R_0}{\sqrt{D}} K_1 \left(\sqrt{\frac{k}{D}} R_0 \right) \right) \quad (6)$$

Proof: The proof of Theorem 3 and Theorem 4 are given in Appendix C. ■

This UCA is accurate if $|\vec{b}|$ is relatively large and thus it is inaccurate when $|\vec{b}| = 0$. The accuracy of the UCA applied in (5) will be verified in Sec. VI.

Remark 1: We have analytically found that $\bar{N}_{\text{agg}}^\dagger(\vec{x}_i, t|\lambda)$ converges as time $t \rightarrow \infty$ when $k \neq 0$, since $\bar{N}_{\text{agg}}^\dagger(\vec{x}_i, t|\lambda) = \sum_{\vec{x}_j \in \Phi(\lambda)} \bar{N}(\vec{x}_i, t|\vec{x}_j)$ and, from (5), $\bar{N}(\vec{x}_i, \infty|\vec{x}_j)$ is a constant when $k \neq 0$. This analytically proves that our assumption adopted for **Reception** in Sec. II is valid, i.e., $\bar{N}_{\text{agg}}^\dagger(\vec{x}_i, t|\lambda)$ does not vary with time t after some time when $k \neq 0$.

Remark 2: We note that $\bar{N}(\vec{b}, \infty) \rightarrow \infty$ when $k = 0$ since $K_0(0) \rightarrow \infty$. Thus, $\bar{N}_{\text{agg}}^\dagger(\vec{x}_i, t|\lambda) = \sum_{\vec{x}_j \in \Phi(\lambda)} \bar{N}(\vec{x}_i, t|\vec{x}_j)$ does not converge as time $t \rightarrow \infty$ when $k = 0$, which will be verified in Sec. VI. Since $\bar{N}(\vec{b}, \infty)$ when $k = 0$ does not converge, we evaluate the time-varying channel response $\bar{N}(\vec{b}, t)$ at time t with no molecule degradation, i.e., $k = 0$, which is given by

$$\bar{N}(\vec{b}, t) \Big|_{k=0} \approx \pi R_0^2 \int_{\tau=0}^t \frac{q}{(4\pi D\tau)} \exp\left(-\frac{|\vec{b}|^2}{4D\tau}\right) d\tau \approx \frac{\Gamma\left(0, \frac{|\vec{b}|^2}{4Dt}\right) q R_0^2}{4D}. \quad (7)$$

B. Randomly-Distributed TXs

In this subsection, we consider that *many* point TXs are randomly distributed over a circle S_1 according to a point process with a constant density λ , as shown in Fig. 1. The circle S_1 is centered at $(0, 0)$ with radius R_1 . We represent \vec{a} as the location of an arbitrary point TX a and $\Phi(\lambda)$ as the set of TXs' random locations. We denote the asymptotic channel response at the circular RX S_0 centered at \vec{b} with radius R_0 , due to continuous emission with rate q since time $t = 0$ from TX a , by $\bar{N}(\vec{b}, \infty|\vec{a})$,

and the corresponding aggregate channel response at the RX due to all randomly-distributed TXs on circle S_1 with density λ by³ $\overline{N}_{\text{agg}}(\vec{b}, \infty|\lambda) = \sum_{\vec{a} \in \Phi(\lambda)} \overline{N}(\vec{b}, \infty|\vec{a})$. We denote $\mathbb{E}_{\Phi} \left\{ \overline{N}_{\text{agg}}(\vec{b}, \infty|\lambda) \right\}$ as the expected $\overline{N}_{\text{agg}}(\vec{b}, \infty|\lambda)$ over the point process $\Phi(\lambda)$. For compactness, we remove ∞ in all notation in the remainder of this paper since we assume that bacteria use asymptotic observations of the continuous emission by TXs to make decisions. We next derive $\mathbb{E}_{\Phi} \left\{ \overline{N}_{\text{agg}}(\vec{b}|\lambda) \right\}$ and simplify it in different special cases in order to ease the computational complexity.

Theorem 5: The expected aggregate channel response at the RX due to all randomly distributed TXs on circle S_1 with density λ over the point process $\Phi(\lambda)$ is given by

$$\begin{aligned} \mathbb{E}_{\Phi} \left\{ \overline{N}_{\text{agg}}(\vec{b}|\lambda) \right\} &= \int_{|\vec{r}|=0}^{R_1} \int_{\varphi=0}^{2\pi} \overline{N}(\vec{b}|\vec{r}) \lambda |\vec{r}| d\varphi d|\vec{r}| \\ &= \lambda \int_{|\vec{r}|=0}^{R_1} \int_{\varphi=0}^{2\pi} \int_{|\vec{r}_0|=0}^{R_0} \int_{\theta=0}^{2\pi} K_0 \left(\sqrt{\frac{k}{D}} \Upsilon(\vec{b}) \right) \frac{q}{2D\pi} |\vec{r}_0| |\vec{r}| d\theta d|\vec{r}_0| d\varphi d|\vec{r}|. \end{aligned} \quad (8)$$

where $\Upsilon(\vec{b})$ is given in $\Upsilon(\vec{b}) = \sqrt{\Omega(\vec{b}) + |\vec{r}_0|^2 + 2\sqrt{\Omega(\vec{b})} |\vec{r}_0| \cos \theta}$ and $\Omega(\vec{b}) = |\vec{b}|^2 + |\vec{r}|^2 + 2|\vec{b}| |\vec{r}| \cos \varphi$.

Proof: See Appendix D. ■

Although we consider a point TX, a circular TX is also of interest since a realistic TX, e.g., a cell, could be approximately spherical and molecules can be generated in different sections throughout a cell. We discuss the channel response due to a circular TX in the following remark:

Remark 3: It can be shown that the asymptotic channel response at a circular RX with radius R_0 centered at \vec{b} , due to continuous emission with rate q from a *circular* TX centered at $(0, 0)$ with radius R_1 since time $t = 0$, can be obtained by removing density λ in (8).

We note that the evaluation of (8) requires very high computational complexity, since it involves four inseparable integrals. Therefore, we simplify (8) for the following corollaries.

Corollary 1 (UCA within RX): When we assume that the concentration within the RX S_0 is uniform, the expected aggregate channel response at the RX $\mathbb{E}_{\Phi} \left\{ \overline{N}_{\text{agg}}(\vec{b}|\lambda) \right\}$ is simplified as

$$\mathbb{E}_{\Phi} \left\{ \overline{N}_{\text{agg}}(\vec{b}|\lambda) \right\} \approx \lambda \int_{|\vec{r}|=0}^{R_1} \int_{\varphi=0}^{2\pi} \frac{qR_0^2}{2D} K_0 \left(\sqrt{\frac{k}{D}} \Omega(\vec{b}) \right) |\vec{r}| d\varphi d|\vec{r}|. \quad (9)$$

³In this paper, N_{agg} and N_{agg}^{\dagger} denote the observation at a RX and at a bacterium, respectively. We use the superscript \dagger to differentiate whether the observation includes the molecules released from itself.

Corollary 2 (RX at Population Circle Center): When the RX is at the center of the circle S_1 where TXs are randomly distributed, the expected aggregate channel response at the RX $\mathbb{E}_\Phi \left\{ \overline{N}_{\text{agg}}(\vec{b}|\lambda) \right\}$ is simplified as

$$\begin{aligned} & \mathbb{E}_\Phi \left\{ \overline{N}_{\text{agg}}(\vec{b}|\lambda) \right\} \Big|_{|\vec{b}|=0} \\ &= \lambda \int_{|\vec{r}|=0}^{R_1} \int_{|\vec{r}_0|=0}^{R_0} \int_{\theta=0}^{2\pi} \frac{q}{D} K_0 \left(\sqrt{\frac{k}{D}} \sqrt{|\vec{r}|^2 + |\vec{r}_0|^2 + 2|\vec{r}||\vec{r}_0| \cos \theta} \right) |\vec{r}_0| |\vec{r}| d\theta d|\vec{r}_0| d|\vec{r}|. \end{aligned} \quad (10)$$

Corollary 3 (RX at Population Circle Center with UCA): When both the concentration within the RX S_0 is uniform and the RX is at the center of the circle S_1 , the expected aggregate channel response at the RX $\mathbb{E}_\Phi \left\{ \overline{N}_{\text{agg}}(\vec{b}|\lambda) \right\}$ is simplified as

$$\mathbb{E}_\Phi \left\{ \overline{N}_{\text{agg}}(\vec{b}|\lambda) \right\} \Big|_{|\vec{b}|=0} \approx \frac{\lambda q \pi R_0^2}{k} \left(1 - \frac{\sqrt{k} R_1 K_1 \left(\sqrt{\frac{k}{D}} R_1 \right)}{\sqrt{D}} \right). \quad (11)$$

Proof: The proofs of Corollary 1, Corollary 2, and Corollary 3 are given in Appendix E. ■

Although (9) cannot be solved in the closed form, (9) is much easier to evaluate than (8). The numerical results in Sec. VI will demonstrate the accuracy of the UCA used in (9).

IV. COOPERATING PROBABILITY AT A FIXED-LOCATION BACTERIUM

In this section, we derive the expected probability of cooperation (i.e., the number of molecules observed from itself and other PPP distributed bacteria is larger than some threshold η) at a bacterium at a fixed location \vec{x}_i over the spatial random point process $\Phi(\lambda)$. We denote such a probability by $\tilde{\Pr}(N_{\text{agg}}^\dagger(\vec{x}_i|\lambda) \geq \eta)$. Please note that in this section \vec{x}_i is a fixed location and does not change in each instantaneous realization of the spatial random point process $\Phi(\lambda)$. In the following, we first derive the exact expression for $\tilde{\Pr}(N_{\text{agg}}^\dagger(\vec{x}_i|\lambda) \geq \eta)$ and then derive an approximate expression. We emphasize that deriving such a probability is challenging since the bacterial locations are different in each realization and the probability of occurrence of realizations needs to be accounted for.

A. Exact Cooperating Probability

In this subsection, we derive the exact expression for $\tilde{\Pr}(N_{\text{agg}}^\dagger(\vec{x}_i|\lambda) \geq \eta)$, i.e.,

$$\tilde{\Pr}(N_{\text{agg}}^\dagger(\vec{x}_i|\lambda) \geq \eta) = \mathbb{E}_\Phi \left\{ \Pr \left(N_{\text{agg}}^\dagger(\vec{x}_i|\lambda) \geq \eta | \overline{N}_{\text{agg}}^\dagger(\vec{x}_i|\lambda) \right) \right\}, \quad (12)$$

where \mathbb{E}_Φ denotes the expectation over the spatial random point process $\Phi(\lambda)$. $N_{\text{agg}}^\dagger(\vec{x}_i|\lambda)$ is the instantaneous observation at the bacterium i and $\overline{N}_{\text{agg}}^\dagger(\vec{x}_i|\lambda)$ is its expected observation for a given instantaneous realization of random bacterial locations. For different realizations of $\Phi(\lambda)$, $\overline{N}_{\text{agg}}^\dagger(\vec{x}_i|\lambda)$

changes in each realization of $\Phi(\lambda)$ since the locations of the PPP distributed bacteria change. In other words, for each realization of Φ , the locations of the PPP distributed bacteria and the resulting $\overline{N}_{\text{agg}}^\dagger(\vec{x}_i|\lambda)$ are random. Therefore, the probability of cooperation in (12) is obtained by averaging the conditional probability $\Pr\left(N_{\text{agg}}^\dagger(\vec{x}_i|\lambda) \geq \eta|\overline{N}_{\text{agg}}^\dagger(\vec{x}_i|\lambda)\right)$ over different realizations of $\Phi(\lambda)$ to capture this randomness.

We note that $N_{\text{agg}}^\dagger(\vec{x}_i|\lambda)$ is a Poisson binomial RV for the following reasons. We recall that $N_{\text{agg}}^\dagger(\vec{x}_i|\lambda)$ is the sum of $N(\vec{x}_i|\vec{x}_j)$ over j . We note that $N(\vec{x}_i|\vec{x}_j)$ is the sum of the number of molecules observed at the bacterium i at time t released from the bacterium j since $t = 0$ s. Thus, the observations at the bacterium i due to continuous emission at the bacterium j are not identically distributed since they are released at different times. Therefore, $N(\vec{x}_i|\vec{x}_j)$ is a Poisson binomial RV since each molecule behaves independently and has a different probability of being observed at $t = t_i^*$ by the bacterium i due to different releasing times. Since $N_{\text{agg}}^\dagger(\vec{x}_i|\lambda)$ is the sum of $N(\vec{x}_i|\vec{x}_j)$, $N_{\text{agg}}^\dagger(\vec{x}_i|\lambda)$ is also a Poisson binomial RV. We note that modeling $N_{\text{agg}}^\dagger(\vec{x}_i|\lambda)$ as a Poisson binomial RV makes the evaluation of (12) very cumbersome. Fortunately, in agreement with our particle-based simulation tests, $N_{\text{agg}}^\dagger(\vec{x}_i, \infty|\lambda)$ can be well approximated as a Poisson RV. Using the Poisson approximations, we rewrite (12) in the following lemma:

Lemma 1: Assuming $N_{\text{agg}}^\dagger(\vec{x}_i|\lambda)$ is a Poisson RV with mean $\overline{N}_{\text{agg}}^\dagger(\vec{x}_i|\lambda)$, the cooperating probability can be written as a function of the Laplace transform of $\overline{N}_{\text{agg}}^\dagger(\vec{x}_i|\lambda)$. The function is given by

$$\tilde{\Pr}\left(N_{\text{agg}}^\dagger(\vec{x}_i|\lambda) \geq \eta\right) = 1 - \sum_{n=0}^{\eta-1} \frac{1}{n!} \left. \frac{\partial^n \mathcal{L}_{\overline{N}_{\text{agg}}^\dagger(\vec{x}_i|\lambda)}(-\rho)}{\partial \rho^n} \right|_{\rho=-1}, \quad (13)$$

where $\mathcal{L}_{\overline{N}_{\text{agg}}^\dagger(\vec{x}_i|\lambda)}(\cdot)$ is the Laplace transform of $\overline{N}_{\text{agg}}^\dagger(\vec{x}_i|\lambda)$, which is defined as $\mathcal{L}_{\overline{N}_{\text{agg}}^\dagger(\vec{x}_i|\lambda)}(s) = \mathbb{E}_\Phi \left\{ \exp \left\{ -s \overline{N}_{\text{agg}}^\dagger(\vec{x}_i|\lambda) \right\} \right\}$.

Proof: See Appendix F. ■

We next derive $\mathcal{L}_{\overline{N}_{\text{agg}}^\dagger(\vec{x}_i|\lambda)}(s)$ in the following lemma.

Lemma 2: We derive $\mathcal{L}_{\overline{N}_{\text{agg}}^\dagger(\vec{x}_i|\lambda)}(s)$ as

$$\mathcal{L}_{\overline{N}_{\text{agg}}^\dagger(\vec{x}_i|\lambda)}(s) = \exp \left\{ -s \overline{N}_{\text{self}} - \lambda \int_{|\vec{r}|=0}^{R_1} \int_{\varphi=0}^{2\pi} (1 - \exp(-s \overline{N}(\vec{x}_i|\vec{r}))) |\vec{r}| d\varphi d|\vec{r}| \right\}, \quad (14)$$

where $\lambda = (\lambda\pi R_1^2 - 1)/\pi R_1^2$ and $\overline{N}(\vec{x}_i|\vec{r})$ is given by

$$\begin{aligned} \overline{N}(\vec{x}_i|\vec{r}) &= \int_{|\vec{r}_0|=0}^{R_0} \int_{\theta=0}^{2\pi} \frac{q}{2D\pi} K_0 \left(\sqrt{\frac{k}{D}} \Upsilon(\vec{x}_i) \right) |\vec{r}_0| d\theta d|\vec{r}_0|, \quad \text{or} \\ \overline{N}(\vec{x}_i|\vec{r}) &\approx \frac{qR_0^2}{2D} K_0 \left(\sqrt{\frac{k}{D}} \Omega(\vec{x}_i) \right). \end{aligned} \quad (15)$$

Proof: See Appendix G. ■

We note that the approximation one in (15) is due to the UCA approximation within S_0 . Using Faà di Bruno's formula [29], we write the n th derivative of $\mathcal{L}_{\overline{N}_{\text{agg}}^\dagger(\vec{x}_i|\lambda)}(-\rho)$ derived in (14) with respect to ρ and then apply it to (13), we obtain

$$\begin{aligned} \tilde{\Pr}(N_{\text{agg}}^\dagger(\vec{x}_i|\lambda) \geq \eta) &= 1 - \mathcal{L}_{\overline{N}_{\text{agg}}^\dagger(\vec{x}_i|\lambda)}(1) \sum_{n=0}^{\eta-1} \sum \frac{1}{\prod_{j=1}^n m_j! j!^{m_j}} \\ &\quad \times \left(\lambda \int_{|\vec{r}|=0}^{R_1} \int_{\varphi=0}^{2\pi} \overline{N}(\vec{x}_i|\vec{r}) \exp(\rho \overline{N}(\vec{x}_i|\vec{r})) |\vec{r}| d\varphi d|\vec{r}| + \overline{N}_{\text{self}} \right)^{m_1} \\ &\quad \times \prod_{j=2}^n \left(\lambda \int_{|\vec{r}|=0}^{R_1} \int_{\varphi=0}^{2\pi} \overline{N}(\vec{x}_i|\vec{r})^j \exp(\rho \overline{N}(\vec{x}_i|\vec{r})) |\vec{r}| d\varphi d|\vec{r}| \right)^{m_j}, \end{aligned} \quad (16)$$

where the sum is over all n -tuples of nonnegative integers (m_1, \dots, m_n) satisfying the constraint $1m_1 + 2m_2 + 3m_3 + \dots + nm_n = n$.

Remark 4: The expression in (16) comprises two integrals and thus (16) cannot be obtained in closed form. However, (16) can be evaluated numerically in a straightforward manner using Mathematica.

B. Approximate Cooperating Probability

In this subsection, we derive an approximate expression for $\tilde{\Pr}(N_{\text{agg}}^\dagger(\vec{x}_i|\lambda) \geq \eta)$ that has lower computational complexity than that of the exact expression derived in (16).

We recall that in (12), we consider the instantaneous realization of $\overline{N}_{\text{agg}}^\dagger(\vec{x}_i|\lambda)$ and its PMF, which makes the evaluation of (12) very complicated. To ease the computational burden, we approximate the instantaneous realization of $\overline{N}_{\text{agg}}^\dagger(\vec{x}_i|\lambda)$ by the expected $\overline{N}_{\text{agg}}^\dagger(\vec{x}_i|\lambda)$ over the spatial random process $\Phi(\lambda)$, $\mathbb{E}_\Phi\{\overline{N}_{\text{agg}}^\dagger(\vec{x}_i|\lambda)\}$, and assume that $N_{\text{agg}}^\dagger(\vec{x}_i|\lambda)$ is a Gaussian or Poisson RV with mean $\mathbb{E}_\Phi\{\overline{N}_{\text{agg}}^\dagger(\vec{x}_i|\lambda)\}$. By doing so, we approximate (12) as:

$$\tilde{\Pr}(N_{\text{agg}}^\dagger(\vec{x}_i|\lambda) \geq \eta) = \mathbb{E}_\Phi \left\{ \Pr \left(N_{\text{agg}}^\dagger(\vec{x}_i|\lambda) \geq \eta | \overline{N}_{\text{agg}}^\dagger(\vec{x}_i|\lambda) \right) \right\} \approx \Pr \left(N_{\text{agg}}^\dagger(\vec{x}_i|\lambda) \geq \eta | \mathbb{E}_\Phi \left\{ \overline{N}_{\text{agg}}^\dagger(\vec{x}_i|\lambda) \right\} \right) \quad (17)$$

By assuming that $N_{\text{agg}}^\dagger(\vec{x}_i|\lambda)$ is a Poisson RV, we further rewrite (17) as

$$\tilde{\Pr}(N_{\text{agg}}^\dagger(\vec{x}_i|\lambda) \geq \eta) = 1 - \frac{\Gamma \left(\eta, \mathbb{E}_\Phi \left\{ \overline{N}_{\text{agg}}^\dagger(\vec{x}_i|\lambda) \right\} \right)}{\Gamma(\eta)}, \quad (18)$$

where $\mathbb{E}_\Phi \left\{ \overline{N}_{\text{agg}}^\dagger(\vec{x}_i|\lambda) \right\}$ is given by

$$\begin{aligned} \mathbb{E}_\Phi \left\{ \overline{N}_{\text{agg}}^\dagger(\vec{x}_i|\lambda) \right\} &= \mathbb{E}_\Phi \left\{ \sum_{\vec{x}_j \in \Phi(\lambda)} \overline{N}(\vec{x}_i|\vec{x}_j) \right\} = \mathbb{E}_\Phi \left\{ \overline{N}(\vec{x}_i|\vec{x}_i) + \sum_{\vec{x}_j \in \Phi(\lambda)/\vec{x}_i} \overline{N}(\vec{x}_i|\vec{x}_j) \right\} \\ &= \overline{N}_{\text{self}} + \mathbb{E}_\Phi \left\{ \sum_{\vec{a} \in \Phi(\lambda)} \overline{N}(\vec{x}_i|\vec{a}) \right\} = \overline{N}_{\text{self}} + \mathbb{E}_\Phi \left\{ \overline{N}_{\text{agg}}(\vec{x}_i|\lambda) \right\}, \end{aligned} \quad (19)$$

where $\mathbb{E}\{\overline{N}_{\text{agg}}(\vec{x}_i|\lambda)\}$ can be obtained by replacing $|\vec{b}|$ with $|\vec{x}_i|$ and λ with λ in (8) if the UCA is not valid or (9) if the UCA is valid.

V. CHARACTERIZATION OF NUMBER OF COOPERATIVE BACTERIA

In this section, we characterize the distribution of the number of cooperators. To this end, we first derive the MGF of the number of cooperators. Using the derived MGF, we then derive the expressions for the moments and cumulants of the number of cooperators. Using the derived moments and cumulants, we study the convergence of the distribution of the number of cooperators to a Gaussian distribution. Furthermore, we derive the expected number of pairs of two nearest bacteria both cooperating, which can be used to study the impact of a cooperative bacterium on the behaviors of the neighboring bacteria in a QS system. The problem addressed in this section is challenging since we need to consider the random received signal at each bacterium in a random location due to the random motion of molecules released from a population of randomly-distributed bacteria.

A. Moment and Cumulant Generating Functions

We denote the decision of cooperation and noncooperation of the bacterium i by $B(\vec{x}_i, \Phi) = 1$ and $B(\vec{x}_i, \Phi) = 0$, respectively. We note that $B(\vec{x}_i, \Phi)$ is a Bernoulli RV with mean $\overline{B}(\vec{x}_i, \Phi)$. We denote the number of all cooperators by Z , i.e., $Z = \sum_{\vec{x}_i \in \Phi(\lambda)} B(\vec{x}_i, \Phi)$. We first derive the exact expression for the MGF of Z and then provide an approximated expression that can be readily used to derive the n th moment and the n th cumulant of Z . We derive the exact expression for the MGF of Z in the following theorem.

Theorem 6: The exact expression for the MGF of Z , $M_Z(u)$, is given by

$$M_Z(u) = \mathbb{E}_\Phi \left\{ \prod_{\vec{x}_i \in \Phi(\lambda)} h(\vec{x}_i, \Phi) \right\}, \quad (20)$$

where $h(\vec{x}_i, \Phi)$ is given by

$$h(\vec{x}_i, \Phi) = 1 + (\exp(u) - 1) \left(1 - \left(\sum_{n=0}^{\eta-1} \frac{1}{n!} \exp \left\{ - \sum_{\vec{x}_j \in \Phi(\lambda)} \overline{N}(\vec{x}_i|\vec{x}_j) \right\} \left(\sum_{\vec{x}_j \in \Phi(\lambda)} \overline{N}(\vec{x}_i|\vec{x}_j) \right)^n \right) \right). \quad (21)$$

Proof: See Appendix H. ■

We note that $h(\vec{x}_i, \Phi)$ not only depends on \vec{x}_i but also depends on the locations of the other bacteria in Φ . Hence, it is mathematically intractable to write $\mathbb{E}\{\prod_{x \in \Phi} h(x, \Phi)\}$ as a form that only includes addition, multiplication, or integrals using existing tools in stochastic geometry, which makes deriving moments or cumulants based on (20) cumbersome. To tackle this problem, we next derive an approximated expression for $M_Z(u)$ in the following theorem.

Theorem 7: The approximated expression for $M_Z(u)$ is given by

$$M_Z(u) \approx \exp\left(-\lambda \int_{|\vec{r}_1|=0}^{R_1} (1 - \exp(u)) \tilde{\Pr}(N_{\text{agg}}^\dagger(\vec{r}_1|\lambda) \geq \eta) 2\pi|\vec{r}_1|d|\vec{r}_1|\right), \quad (22)$$

where $\tilde{\Pr}(N_{\text{agg}}^\dagger(\vec{r}_1|\lambda) \geq \eta)$ can be obtained by replacing \vec{x}_i with \vec{r}_1 in (16) or (18). We also derive the approximated cumulant generating function of Z , $\mathcal{K}_Z(u)$, as

$$\mathcal{K}_Z(u) \approx -\lambda \int_{|\vec{r}_1|=0}^{R_1} (1 - \exp(u)) \tilde{\Pr}(N_{\text{agg}}^\dagger(\vec{r}_1|\lambda) \geq \eta) 2\pi|\vec{r}_1|d|\vec{r}_1|. \quad (23)$$

Proof: See Appendix I. ■

We discuss the accuracy of the approximation in (22) and (23) in the following remark:

Remark 5: Based on Appendix I, the approximation in (22) and (23) is because we use the expected cooperating probability over the spatial point process Φ to approximate the conditional cooperating probability for a given instantaneous realization of this point process Φ . Intuitively, this approximation is more accurate when the density of the bacterial population, λ , is lower. This is because when the density is lower, the instantaneous number of received molecules from other bacteria is closer to the expected number of received molecules over the spatial point process Φ . Hence, the cooperating probability for a given instantaneous realization of Φ is closer to that expected over Φ , thus the approximation is more accurate. The numerical results in Sec. VI will verify this intuition.

B. Moments, Cumulants, and Distribution

We derive the n th moment of Z and the n th cumulant of Z in the following theorem.

Theorem 8: The expression for the n th moment of Z is given by

$$\mathbb{E}_\Phi\{(Z)^n\} \approx \sum \frac{n!}{\prod_{j=1}^n m_j! j!^{m_j}} \prod_{j=1}^n \left(\lambda \int_{|\vec{r}_1|=0}^{R_1} \tilde{\Pr}(N_{\text{agg}}^\dagger(\vec{r}_1|\lambda) \geq \eta) 2\pi|\vec{r}_1|d|\vec{r}_1| \right)^{m_j}, \quad (24)$$

where the sum is over all n -tuples of nonnegative integers (m_1, \dots, m_n) satisfying the constraint $1m_1 + 2m_2 + 3m_3 + \dots + nm_n = n$. The expression for the n th cumulant of Z , denoted by $\kappa(n)$, is given by

$$\kappa(n) \approx \lambda \int_{|\vec{r}_1|=0}^{R_1} \tilde{\Pr}(N_{\text{agg}}^\dagger(\vec{r}_1|\lambda) \geq \eta) 2\pi|\vec{r}_1|d|\vec{r}_1|. \quad (25)$$

Proof: (24) can be obtained by $\mathbb{E}_\Phi\{(Z)^n\} = \frac{\partial^n M_Z(u)}{\partial u^n} \Big|_{u=0}$ and Faà di Bruno's formula. (25) can be obtained by $\kappa(n) = \frac{\partial^n \mathcal{K}_Z(u)}{\partial u^n} \Big|_{u=0}$ and the expression for $\mathcal{K}_Z(u)$ derived in (23). ■

Based on (24), we have the following propositions about the moments of Z :

Proposition 2: The approximation of the first moment of Z , $\mathbb{E}_\Phi\{Z\}$, given by (24) is tight, i.e.,

$$\mathbb{E}_\Phi\{Z\} = \lambda \int_{|\vec{r}_1|=0}^{R_1} \tilde{\Pr}(N_{\text{agg}}^+(\vec{r}_1|\lambda) \geq \eta) 2\pi |\vec{r}_1| d|\vec{r}_1|. \quad (26)$$

Proof: See Appendix J. ■

Proposition 3: When the density of the bacterial population, λ , is relatively low, the variance of Z , denoted by $\text{Var}\{Z\}$, can be well approximated by its mean $\mathbb{E}_\Phi\{Z\}$, i.e.,

$$\text{Var}\{Z\} \approx \mathbb{E}_\Phi\{Z\}. \quad (27)$$

Proof: Applying $n = 2$ to (24) and combining with (26), we obtain the second moment of Z as $\mathbb{E}_\Phi\{(Z)^2\} \approx (\mathbb{E}_\Phi\{Z\})^2 + \mathbb{E}_\Phi\{Z\}$. Using this relation and $\text{Var}\{Z\} = \mathbb{E}_\Phi\{(Z)^2\} - (\mathbb{E}_\Phi\{Z\})^2$, we obtain $\text{Var}\{Z\} \approx \mathbb{E}_\Phi\{Z\}$. In addition, as discussed in Remark 5, the approximation used in (22) and (23) is more accurate when the density λ is lower. This complete the proof. ■

Interestingly, by combining (24), (26), and (25), we obtain the relation between $\mathbb{E}_\Phi\{(Z)^n\}$, $\mathbb{E}_\Phi\{Z\}$, and $\kappa(n)$, as follows:

$$\mathbb{E}_\Phi\{(Z)^n\} \approx \sum \frac{n!}{\prod_{j=1}^n m_j! j!^{m_j}} \prod_{j=1}^n (\mathbb{E}_\Phi\{Z\})^{m_j}, \quad \kappa(n) \approx \mathbb{E}_\Phi\{Z\}. \quad (28)$$

Thus, once $\mathbb{E}_\Phi\{Z\}$ in (26) is determined, $\mathbb{E}_\Phi\{(Z)^n\}$ and $\kappa(n)$ can be easily determined via (28).

We discuss the effect of motion of bacteria on the number of cooperators in the following remark:

Remark 6: If we assume bacteria experience unbiased diffusive motion over time after being randomly placed, our simulation results (see Appendix L) show that the number of cooperators would decrease as the bacteria's diffusion coefficient increases (i.e., as bacteria move faster). This is because when bacteria move faster, the distance between bacteria is larger and they observe fewer molecules, which leads to a smaller cooperation probability and fewer cooperators.

We finally investigate the distribution of the number of cooperators, Z . The skewness and kurtosis describe the symmetry and peakedness of the distribution of a RV, respectively. Using (25) and [30], we derive the skewness, β_1 and kurtosis, β_2 , of Z as

$$\beta_1 = \frac{\kappa(3)}{\kappa(2)^{3/2}} \approx (\mathbb{E}_\Phi\{Z\})^{-\frac{1}{2}}, \quad \beta_2 = \frac{\kappa(4)}{\kappa(2)^2} \approx (\mathbb{E}_\Phi\{Z\})^{-1}. \quad (29)$$

Based on [31], the skewness and kurtosis together can be employed to assess the normality of a distribution. For a Gaussian distribution, $\beta_1 = \beta_2 = 0$. Thus, if both $\beta_1 \rightarrow 0$ and $\beta_2 \rightarrow 0$, we can say

that the RV could be closely approximated by a Gaussian distribution [32]. Based on (29), we see that Z can be approximated by a Gaussian distribution when $\mathbb{E}_\Phi\{Z\} \rightarrow \infty$ since $\mathbb{E}_\Phi\{Z\} \rightarrow \infty$ leads to $\beta_1 \rightarrow 0$ and $\beta_2 \rightarrow 0$. Using $\mathbb{E}_\Phi\{Z\}$ and $\text{Var}\{Z\}$ derived in this subsection, we can use well-known closed-form distributions (e.g., Poisson and Gaussian distributions) to approximate the PMF and CDF of Z . In Sec. VI, we will use Poisson and Gaussian distributions with derived mean and variance to fit the PMF and CDF of the number of cooperators.

C. Pairs of Two Nearest Bacteria Both Cooperating

Using the cooperating probability derived in Section IV, we evaluate the expected number of pairs of one node and its n th nearest node to both be cooperators, which we denote by $P(n)$. Such an expression can be used to quantify the average number of clusters of cooperators and to study the impact of a cooperative bacterium on the cooperative behaviors of its neighbors. For example, we could compare the number of pairs of two nearest bacteria both cooperating and the number of cooperators derived in Section V.B to know whether most cooperators are the only cooperators in their vicinity, which shows the impact of a cooperative bacterium on the behaviors of its neighbors. We first write $P(n)$ as

$$P(n) = \mathbb{E}_\Phi \left\{ \sum_{\vec{x}_i \in \Phi(\lambda)} \{ \Pr(B(\vec{x}_i, \Phi) = 1) \Pr(B(\vec{x}_{i,n}, \Phi) = 1) \} \right\}, \quad (30)$$

where $\vec{x}_{i,n}$ is the n th nearest node to node \vec{x}_i . We derive $P(n)$ in the following theorem.

Theorem 9: The expression of $P(n)$ is given by

$$P(n) = \lambda \int_{|\vec{r}_1|=0}^{R_1} \left\{ \tilde{\Pr}(N_{\text{agg}}^\dagger(\vec{r}_1|\lambda) \geq \eta) \int_{|\vec{r}_2|=0}^{R_1} \int_{\psi=0}^{2\pi} \tilde{\Pr}(N_{\text{agg}}^\dagger(\vec{r}_2|\lambda) \geq \eta) \frac{g_n(r(\vec{r}_1))}{2\pi r(\vec{r}_1)} |\vec{r}_2| d|\vec{r}_2| d\psi \right\} 2\pi |\vec{r}_1| d|\vec{r}_1|, \quad (31)$$

where $\tilde{\Pr}(N_{\text{agg}}^\dagger(\vec{x}|\lambda) \geq \eta)$ can be obtained by replacing \vec{x}_i with \vec{x} in (16) or (18).

Proof: See Appendix K. ■

VI. NUMERICAL RESULTS AND SIMULATIONS

In this section, we present simulation and numerical results to assess the accuracy of our derived analytical results and reveal the impact of environmental parameters on the number of molecules observed, the cooperating probability, and the statistics of the number of cooperators derived in Sections III–V.

The simulation details are as follows. The simulation environment is unbounded. We vary density, bacteria community radius R_1 , and threshold η . Unless specified otherwise, we consider molecule

degradation with rate $k = 1 \times 10^1/\text{s}$ in the environment, a circular RX with $R_0 = 0.757 \mu\text{m}$, emission rate $q = 1 \times 10^3 \text{ molecule/s}$, and diffusion coefficient $D = 5.5 \times 10^{-10} \text{m}^2/\text{s}$. The values of environment parameters are chosen to be on the same orders as those used in [21]–[23], [33]. In particular, the chosen value of D is the diffusion coefficient of the 3OC6-HSL in water at room temperature [33]. The volume of a sphere with the chosen radius is approximately equal to the volume of *V. fischeri*⁴. We emphasize that these parameters are example values and the general trends of our numerical observations in the following figures do not change for other combinations of parameter values. We simulate the Brownian motion of molecules using a particle-based method as described in [34]. The molecules are initialized at the center of bacteria. The location of each molecule is updated every time step Δt , where diffusion along each dimension is simulated by generating a normal RV with variance $2D\Delta t$. Every molecule has a chance of degrading in every time step with the probability $\exp(-k\Delta t)$. In simulations, the locations of bacteria are randomly generated according to a 2D PPP, thus the number of bacteria in different realizations is a Poisson RV and we consider that the average number of TXs or bacteria is 100 in Figs. 5–11. Since the time between consecutive events in a 1D PPP is exponentially distributed, we generate i.i.d. exponential RVs for each bacterium to simulate the time between consecutive molecule releases. There are also other methods to generate random release times, e.g., we could generate Poisson RVs as the numbers of release times within a fixed time duration and then uniformly distribute these release times over the fixed duration. In Fig. 4, there is one TX at a fixed location and for each realization we randomly generate molecule release times at the TX. In Figs. 5–11, for each realization we randomly generate both the locations and molecule release times for all TXs (bacteria).

In Fig. 4, we plot the expected number of molecules observed at the RX due to one TX's impulse emission with 10^6 molecules in Fig. 4(a) and one TX's continuous emission in Fig. 4(b). The analytical curves in Case i)–Case v) are obtained by (3), (4), (5), (7), and (6), respectively. In Fig. 4(a), we see that there is an optimal time at which channel response is maximal when the RX is not at the TX, while the channel response always decreases with time when the RX is at the TX. This is not surprising since the molecules diffuse away once released. In Fig. 4(b), we see that the channel response with molecular degradation converges as time goes to infinity, while the channel response without molecular degradation always increases with time.

⁴In fact, the shape of *V. fischeri* is a straight rod that is $0.8 \mu\text{m}$ – $1.3 \mu\text{m}$ in diameter and $1.8 \mu\text{m}$ – $2.4 \mu\text{m}$ in length. Due to its rod shape, we calculate its average volume as $\pi(((0.8 \mu\text{m} + 1.3 \mu\text{m})/2)/2)^2(1.8 \mu\text{m} + 2.4 \mu\text{m})/2 = 1.82 \mu\text{m}^3$. Thus, we choose $R_0 = 0.757 \mu\text{m}$ which satisfies $(4/3)\pi R_0^3 = 1.82 \mu\text{m}^3$.

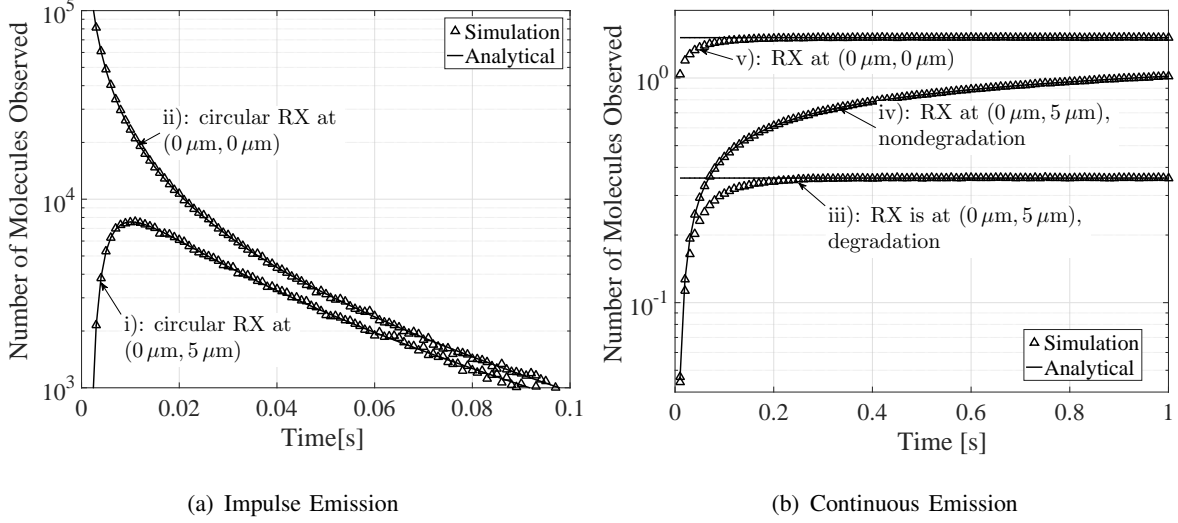


Fig. 4. The expected number of molecules observed at the RX $\bar{N}(\vec{b}, t)$ versus time due to the emission of one TX located at $(0, 0)$. In Fig. 4(a), we consider one *impulse emission* with 10^5 molecules and molecular degradation is considered. We consider two cases of the RX in Fig. 4(a): Case i) the circular RX located at $(0, 5 \mu\text{m})$ and Case ii) the circular RX located at $(0, 0)$. In Fig. 4(b), we consider continuous emission and the circular RX is considered. We consider three cases of the RX in Fig. 4(b): Case iii) the RX located at $(0, 5 \mu\text{m})$ with molecular degradation, Case iv) the RX located at $(5 \mu\text{m}, 0)$ without molecular degradation, and Case v) the RX located at $(0, 0)$ with molecular degradation.

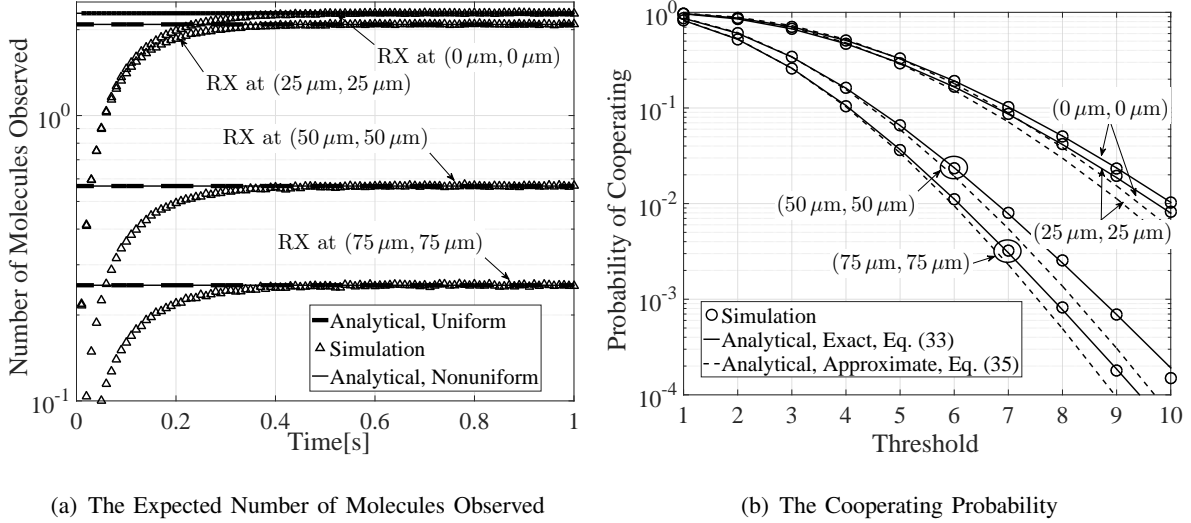


Fig. 5. The expected number of molecules observed at the RX, $\mathbb{E}_{\Phi} \left\{ \bar{N}_{\text{agg}}(\vec{b}|\lambda) \right\}$, in Fig. 5(a) and the corresponding cooperating probability at the RX, $\tilde{\text{Pr}} \left(N_{\text{agg}}^{\dagger}(\vec{x}_i|\lambda) \geq \eta \right)$, in Fig. 5(b) due to continuous emission at randomly-distributed TXs. For different environmental radii $R_1 = 50 \mu\text{m}$, $R_1 = 100 \mu\text{m}$, and $R_1 = 150 \mu\text{m}$, the RX's location is $(\frac{R_1}{2}, \frac{R_1}{2})$. For $R_1 = 50 \mu\text{m}$, we also consider the RX located at the center of environment, i.e., $(0, 0)$.

In Fig. 5, we plot the expected number of molecules observed at the RX in Fig. 5(a) and the corresponding cooperating probability at the RX in Fig. 5(b) due to continuous emission at randomly-distributed TXs for different environmental radii. We first discuss the results in Fig. 5(a). The asymptotic curves when the RX is at $(0, 0)$ with the UCA and without UCA are obtained by (11)

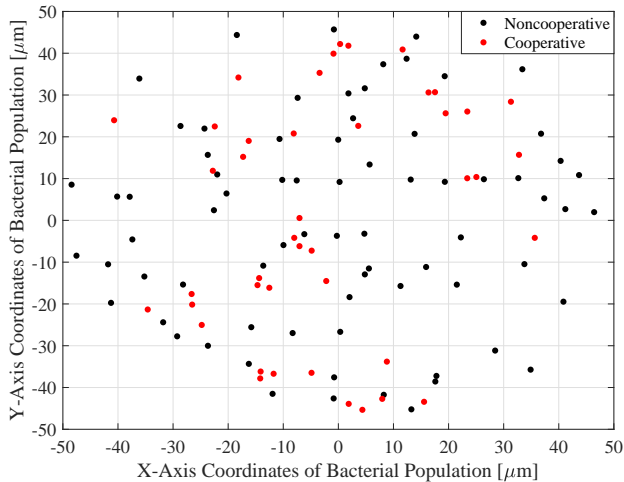


Fig. 6. A realization of a 2D PPP of randomly-distributed bacteria and the resulting cooperative bacteria. $R_1 = 50 \mu\text{m}$.

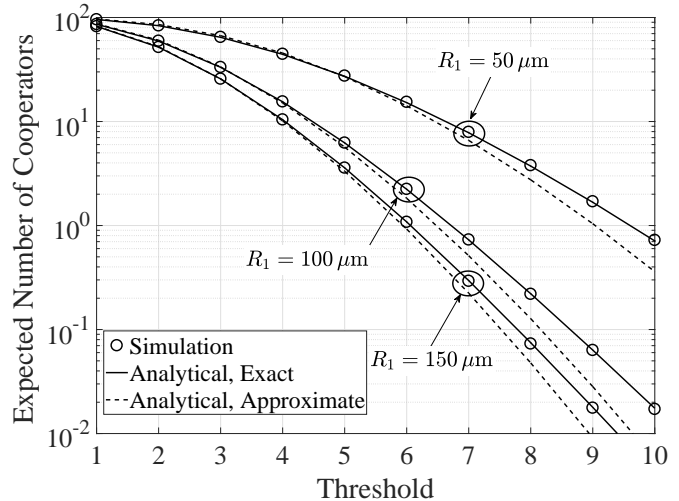


Fig. 7. The expected number of cooperators over spatial PPP $\mathbb{E}_\Phi\{Z\}$ versus threshold η for different population radii R_1 .

and (10), respectively. The asymptotic curves when the RX is at $(\frac{R_1}{2}, \frac{R_1}{2})$ with UCA and without UCA are obtained by (9) and (8), respectively. As observed in Fig. 4(b), we see that the expected number of molecules observed in Fig. 5(a) first increases with time and then becomes stable after some time. We then see that the asymptotic curves with UCA and without UCA almost overlap with each other. This demonstrates the accuracy of the UCA in the derivation of the asymptotic channel response where a circular field of TXs continuously emits molecules.

Next, we discuss the results in Fig. 5(b). The exact and approximate analytical curves are obtained by (16) via (E.1) and (18) via (9), respectively. We see that (16) is always accurate while (18) is only accurate when the probability of cooperation is relatively high, e.g., $\tilde{\Pr}(N_{\text{agg}}^+(\vec{x}_i|\lambda) \geq \eta) \geq 10^{-1}$. We note that the computational complexity of (18) is much lower than that of (16). Thus, in the circumstances of limited computational capabilities and high probability of cooperation, (18) is a good method to estimate the probability of cooperation. Finally, we note that when R_1 decreases, the expected number of molecules and the probability of cooperation increase. This is because the density of TXs is higher when R_1 is smaller.

In Fig. 6, we simulate the decisions of bacteria under one realization of randomly-distributed bacteria locations and random molecule release times at all bacteria. We plot the spatial distribution of cooperators in this realization. In Fig. 7, we plot the first moment (i.e, the mean) of the number of cooperative bacteria versus threshold for different population radii. The exact analytical curves are obtained by (26) via (16) and (E.1) and the approximate analytical curves are obtained by (26) via (18) and (9). We see that the curves obtained by (26) via (18) are only accurate when $\mathbb{E}_\Phi\{Z\} \geq 10$.

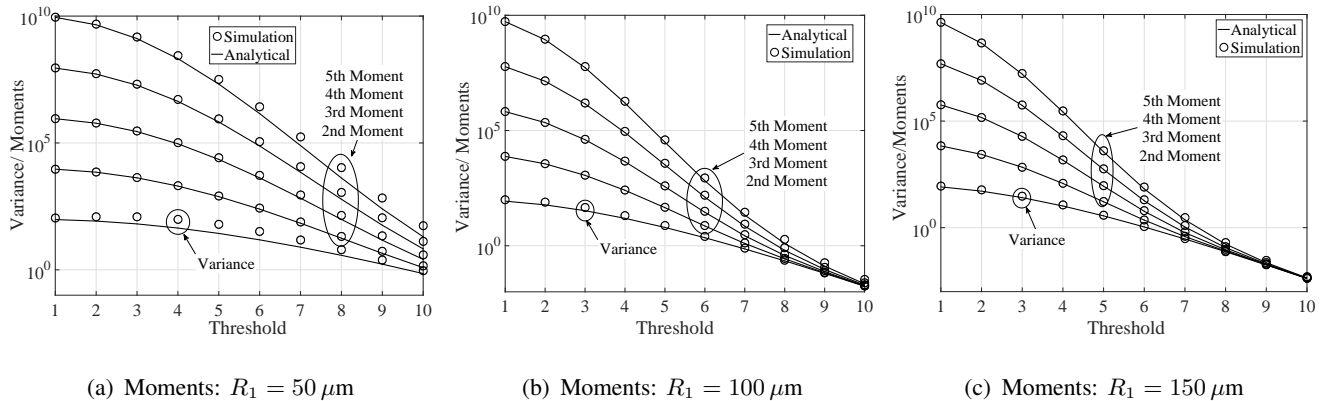


Fig. 8. The different orders of moments of number of cooperators $\mathbb{E}_\Phi\{(Z)^n\}$ versus threshold η for different population radii R_1 .

TABLE I

DEVIATION BETWEEN SIMULATION AND ANALYTICAL VALUES AT PEAK PMF IN FIG. 9.

	(a)	(b)	(c)	(d)	(e)	(f)
Poisson Approximation	6.01%	5.09%	6.02%	45.42%	9.65%	1.77%
Gaussian Approximation	6.01%	5.09%	6.04%	48.23%	10.20%	4.01%

This is because (18) is only accurate when $\tilde{\Pr}(N_{\text{agg}}^\dagger(\vec{x}_i|\lambda) \geq \eta) \geq 10^{-1}$, as observed in Fig. 5(b). We also see that the analytical mean obtained by (26) via (16) exactly matches with simulations. This observation numerically validates Remark 3, i.e., the approximation in (I.1) is tight for the first moment of the number of cooperators. We also see that the expected number of cooperators decreases when the threshold increases, because the probability of cooperation is smaller when the threshold is higher, as observed in Fig. 5(b).

In Figs. 8(a)–8(c), we plot the variance and moments of number of cooperators versus threshold for different population radii. The analytical variances are obtained by (27) and the analytical moments are obtained by (28) via (26). We first see that when the population density is smaller (i.e., R_1 is larger), the accuracy of the analytical variances and the moments improves, thereby validating Remark 3. We then see that the curves of different moments of number of cooperators merge as the threshold increases. This can be explained by the extreme case that the different moments of the number of cooperators would tend to zero as the threshold continually increases, leading to the fact that different moments of the number of cooperators become the same as the threshold continually increases.

We investigate the distributions of the simulated number of cooperators using the statistical distribution fitting software EasyFit⁵. We find that the simulated number of cooperators can be generally well fitted by Beta, Johnson SB, Normal (Gaussian), and Gamma distributions when the number of

⁵ <http://www.mathwave.com/easyfit-distribution-fitting.html>

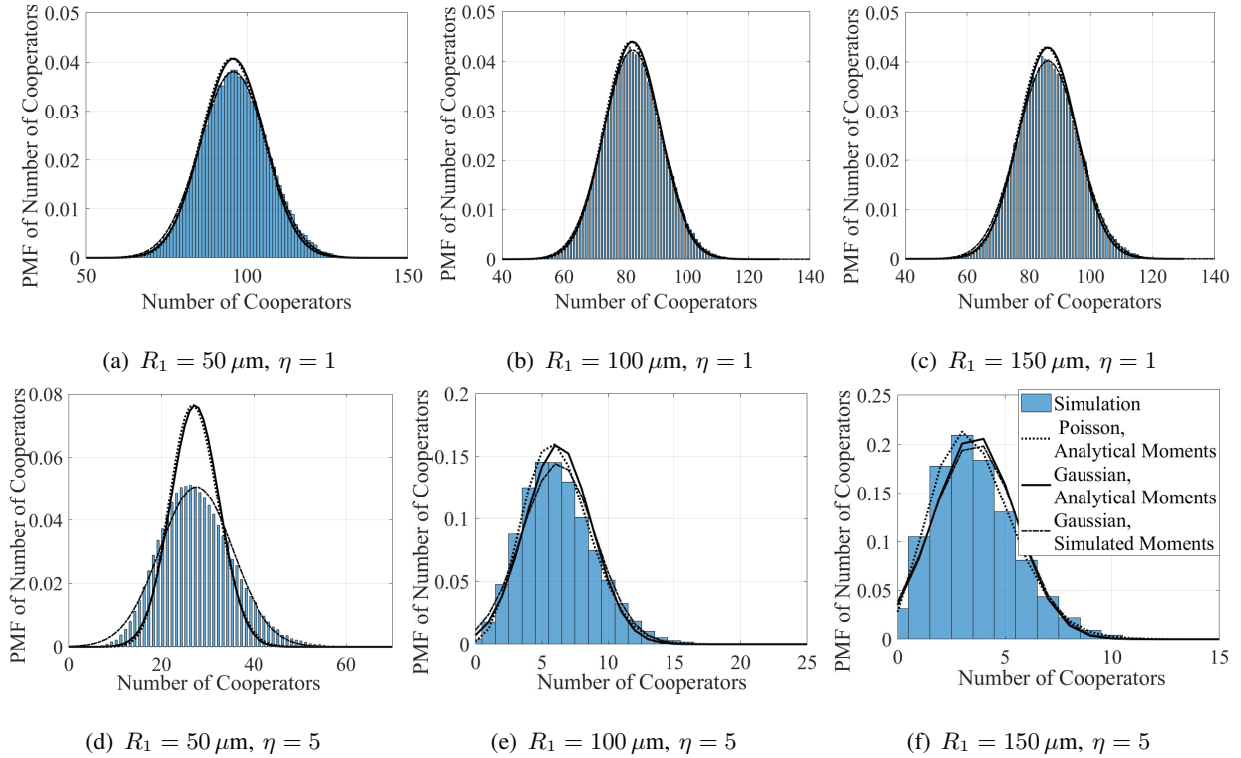


Fig. 9. The PMF of number of cooperators for different population radii R_1 and different thresholds η .

cooperators is large. When the number of cooperators is small, the simulated number of cooperators can be generally well fitted by Poisson and Binomial distributions. We note that Gaussian and Poisson distributions are the most convenient distributions among them while achieving good fitting accuracy. Hence, we use the Gaussian and Poisson distributions with our derived mean and variance to analytically fit the simulated distribution of cooperators in Fig. 9 for assessing its accuracy to analytically predict the distribution of cooperators.

In Fig. 9, we use the Poisson and Gaussian distributions with analytical mean $\mathbb{E}_\Phi\{Z\}$ and variance $\text{Var}\{Z\}$ shown in Fig. 8 to fit the PMF of simulated number of cooperators. To quantitatively assess the accuracy of Poisson and Gaussian approximations, we calculate the deviation between the simulation and analytical curves by $|\text{analysis} - \text{simulation}|/\text{simulation}$. We are interested in the deviation at the peak PMF since such deviation is the largest difference across the whole range of the PMF. The calculated deviation for different cases in Fig. 9 is listed in Table I. Based on Table I, we see that the distribution of the number of cooperators can generally be well approximated by the Poisson and Gaussian distributions, especially when the expected number is relatively large, which meets our expectations discussed in Sec. V-B. When the number of cooperators is relatively small, e.g., $Z < 15$, the Poisson approximation has better accuracy than the Gaussian approximation. This observation is also expected since the continuous Gaussian distribution is an approximation of the

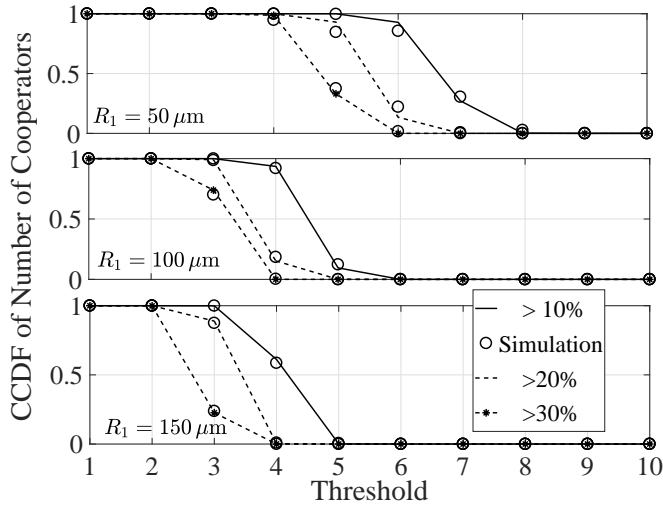


Fig. 10. The CCDF that the number of cooperators versus threshold η for different population radii R_1 .

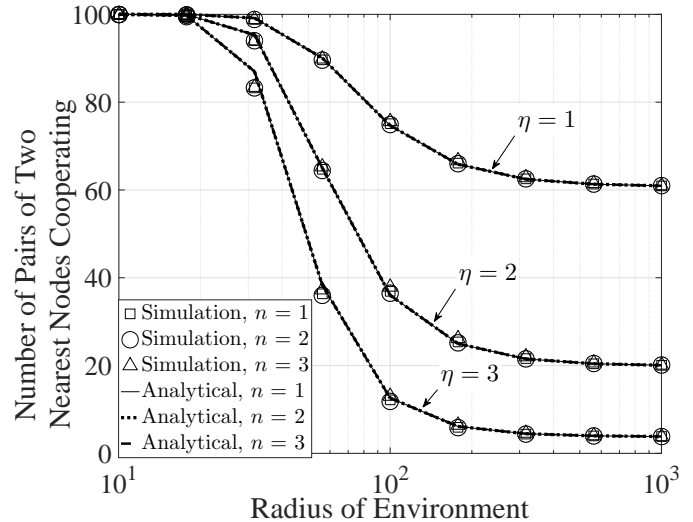


Fig. 11. The number of pairs of any node and its n th nearest node both cooperating versus the population radius.

discrete distribution and such approximation is more accurate when the number of cooperators is higher. The deviation between the Poisson and Gaussian distributions and simulated distribution for $R_1 = 50 \mu\text{m}$ and $\eta = 5$ is caused by the deviation between the analytical variance and simulated variance, as observed in Fig. 8(a).

In Fig. 10, we plot the complementary CDF (CCDF) of the number of cooperators versus threshold for different population radii. These CCDFs could be interpreted as the probability of success to activate a colony of bacteria if we can define the activation of the colony as a minimal number of cells (i.e., fraction of the colony) being activated. The probability of success indicates the overall activation level of a colony, e.g., the likelihood of the colony forming a biofilm. The analytical curves are obtained by the CCDF of the Poisson distribution with analytical mean $\mathbb{E}_{\Phi}\{Z\}$ and variance $\text{Var}\{Z\}$ shown in Fig. 8, respectively. We see that the CCDF of the number of cooperators can be well approximated by that of the Poisson distributions. We also see that the CCDF of the number of cooperators decreases as the threshold increases. The PMF and CDF in Figs. 9 and 10 indicates that the Poisson and Gaussian approximations can be used to not only accurately model the distribution of the number of observed molecules as many MC works have done, e.g., [25], [35], [36], but also model the distribution of the number of cooperative bacteria in QS with good accuracy. Therefore, the easy-to-use Poisson and Gaussian distributions with our derived mean and variance serve as powerful tools to predict the group behavior of bacteria in QS and control their group behavior by adjusting the environmental parameters, e.g., diffusion coefficient and chemical reaction rate. Thus, our research plays as an important role in advancing numerous QS-related healthcare and environmental

applications, e.g., preventing the formation of biofilms in antibiotic resistance and understanding the bioluminescence in environmental monitoring.

In Fig. 11, we plot the number of pairs of any node and its n th nearest node both cooperating $P(n)$ versus the population radius R_1 for different thresholds η . The analytical curves are obtained by (31). We first see that for the same threshold η , the curves of $P(n)$ with different n almost overlap. This is because bacteria are randomly distributed and the observations among different bacteria are independent. This observation is not intuitive, which suggests that the distance between bacteria has a minor impact on the average number of clusters of cooperators. Second, we see that the curves of $P(n)$ first decrease and then converge to a constant number as the population radius R_1 increases. This is because when the population radius increases, the number of molecules observed by the bacteria decreases, but as the population radius tends to infinity, the molecules received by any bacterium is dominated by the molecules released from itself and the number of molecules received by any bacterium converges to a constant number. This observation suggests that the density of bacteria has a marginal impact on the average number of clusters of cooperators when the density is very low.

VII. CONCLUSIONS

In this work, we provided an analytically-tractable model for predicting the concentration of molecules observed by bacteria and the statistics of the number of responsive cooperative bacteria, by taking the motion of molecules undergoing independent diffusion and degradation into consideration. We adopted some assumptions to capture the basic features of QS, e.g., random bacterial location, random molecular emission times, and each bacterium both acting as a TX and a RX. Upon these realistic assumptions, the 2D channel response and the expected probability of cooperation at a bacterium due to continuous emission of molecules at randomly-distributed bacteria were derived. The different order moments and cumulants, the CDF and PMF of the number of cooperators, and the number of pairs of two bacteria both cooperating, were also derived. Since we considered molecular propagation channels among a population of bacteria, the impact of environmental factors on the QS process could be predicted, e.g., environment temperature and pH can affect the diffusion coefficient and degradation rate, respectively.

Interesting future works include relaxing these simplifications, and validating our theoretical model using lab experiments in a 2D environment. Potential experimental setups for validation may include bacteria strains in plastic Petri dishes, bioluminescence monitoring systems that detect cooperative bacteria concentrations by their light emission [37], and computers for post-processing and analysis. Modeling multiple species of bacteria in QS is also interesting future work since multispecies QS

signals may inhibit quorum sensing activation [2]. For example, some types of bacteria produce enzymes that destroy quorum sensing signals of other types of bacteria. Such inhibition could lead to lower cooperative probabilities and fewer cooperators compared to the case when QS is in the absence of the bacteria that release the destructive enzymes. Finally, we note that our analytically-tractable model could be readily extended to a three-dimensional (3D) environment by changing the 2D area integrations to 3D volume integrations.

APPENDIX A

PROOF OF PROPOSITION 1

To prove (2), we have

$$\overline{N}(\vec{b}, t) \stackrel{(a)}{=} \mathbb{E} \left\{ \sum_{\tau \in [0, t]} \overline{N}_{\text{im}}(\vec{b}, t - \tau) \right\} \stackrel{(b)}{=} q \int_{\tau=0}^t \overline{N}_{\text{im}}(\vec{b}, t - \tau) d\tau \stackrel{(c)}{=} q \int_{\tau=0}^t \overline{N}_{\text{im}}(\vec{b}, \tau) d\tau, \quad (\text{A.1})$$

where $\overline{N}_{\text{im}}(\vec{b}, t - \tau)$ is the channel response observed at time t due to the one molecule emitted at time τ and τ is a random time instant on a real line $[0, t]$ distributed according to a 1D PPP with density (rate) q . Equality (a) exploits the fact that the channel response at time t due to *continuous* emission is equal to the expected sum of all channel responses due to all impulse emissions at different random time instants. Equality (b) is obtained by applying Campbell's Theorem and equality (c) is obtained by applying a variable transformation. By taking the limit $t \rightarrow \infty$ in (A.1), we obtain (2).

APPENDIX B

PROOF OF THEOREM 1 AND THEOREM 2

To prove (3), we have

$$\begin{aligned} \overline{N}_{\text{im}}(\vec{b}, \tau) &\stackrel{(a)}{=} \int_{r=0}^{R_0} \int_{\theta=0}^{2\pi} C(\vec{r}_1, \tau) r d\theta dr = \int_{r=0}^{R_0} \int_{\theta=0}^{2\pi} \frac{1}{(4\pi D\tau)} \exp\left(-\frac{|\vec{r}_1|^2}{4D\tau} - k\tau\right) r d\theta dr \\ &= \int_{r=0}^{R_0} \int_{\theta=0}^{2\pi} \frac{1}{(4\pi D\tau)} \exp\left(-\frac{|\vec{b}|^2 + r^2 + 2|\vec{b}|r \cos\theta}{4D\tau} - k\tau\right) r d\theta dr \\ &\stackrel{(b)}{=} \frac{1}{4\pi D} \exp(-k\tau) \int_{r=0}^{R_0} \frac{r}{\tau} \exp\left(-\frac{|\vec{b}|^2 + r^2}{4D\tau}\right) 2\pi I_0\left(\frac{|\vec{b}|r}{2D\tau}\right) dr \\ &\stackrel{(c)}{\approx} \sum_{i=1}^4 \left\{ \frac{1}{2D} \exp(-k\tau) \int_{r=0}^{R_0} \frac{r}{\tau} \exp\left(-\frac{|\vec{b}|^2 + r^2}{4D\tau}\right) \alpha_i \exp\left(\beta_i \frac{|\vec{b}|r}{2D\tau}\right) dr \right\} \quad (\text{B.1}) \end{aligned}$$

where $C(\vec{r}, \tau) = \frac{1}{(4\pi D\tau)} \exp\left(-\frac{|\vec{r}|^2}{4D\tau} - k\tau\right)$ [38, eq. (3.4)] is the channel response at the point defined by \vec{r} at the time τ due to an impulse emission of one molecule from the point at $(0, 0)$ at time $\tau = 0$ into an unbounded 2D environment. Equality (a) is due to the fact that $\overline{N}_{\text{im}}(\vec{b}, \tau)$ for a circular

passive observer S_0 centered at \vec{b} can be obtained by integrating $C(\vec{r}_1, \tau)$ over S_0 , where \vec{r}_1 is a vector from $(0, 0)$ to a point within the RX S_0 . Equality (b) is obtained by applying [17, eq. (3.339)] and equality (c) is obtained by applying $I_0(z) \approx \sum_{i=1}^4 \alpha_i \exp(\beta_i z)$ [27, eq. (7)]. Calculating the final expression of (B.1), we obtain (3). To prove (4), we simplify (B.1) using $|\vec{b}| = 0$ as

$$\bar{N}_{\text{im,self}}(\tau) = \int_{r=0}^{R_0} \int_{\theta=0}^{2\pi} \frac{\exp\left(-\frac{r^2}{4D\tau} - k\tau\right)}{(4\pi D\tau)} d\theta dr = \int_{r=0}^{R_0} \frac{r}{(2D\tau)} \exp\left(-\frac{r^2}{4D\tau} - k\tau\right) dr. \quad (\text{B.2})$$

We then apply [17, eq. (2.33.12)] to (B.2) to solve it as (4), which completes the proof.

APPENDIX C

PROOF OF THEOREM 3 AND THEOREM 4

We first prove (5). Based on (2), the channel response due to continuous emission in (5) can be obtained by integrating the impulse channel response over time, but integrating (3) over τ incurs very high complexity. Thus, we simplify (3) by considering UCA within the circular RX. i.e., $\bar{N}_{\text{im}}(\vec{b}, \tau) \approx \pi R_0^2 C(\vec{b}, \tau)$. Based on (2) and the UCA, we evaluate $\bar{N}(\vec{b}, \infty)$ as

$$\bar{N}(\vec{b}, \infty) \approx \pi R_0^2 \int_{\tau=0}^{\infty} q C(\vec{b}, \tau) d\tau \approx \pi R_0^2 q \int_{\tau=0}^{\infty} \frac{1}{(4\pi D\tau)} \exp\left(-\frac{|\vec{b}|^2}{4D\tau} - k\tau\right) d\tau. \quad (\text{C.1})$$

We then employ $\int_0^{\infty} x^{\nu-1} \exp(-\frac{\beta}{x} - \gamma x) dx = 2 \left(\frac{\beta}{\gamma}\right)^{\frac{\nu}{2}} K_{\nu}(2\sqrt{\beta\gamma})$ [17, eq. (3.471)] to solve (C.1) as (5). To prove (6), we apply (4), $\int_0^{\infty} \exp(-px) dx = 1/p$ [17, eq. (3.310)], and $\int_0^{\infty} \exp(-\frac{\beta}{x} - \gamma x) dx = \frac{\beta}{\gamma} K_1(\sqrt{\beta\gamma})$ [17, eq. (3.324.1)] to (2), we evaluate $\bar{N}_{\text{self}}(\infty)$ as (6). This completes the proof.

APPENDIX D

PROOF OF THEOREM 5

Using Campbell's theorem [39], we first write

$$\mathbb{E}_{\Phi} \left\{ \bar{N}_{\text{agg}}(\vec{b}|\lambda) \right\} = \mathbb{E}_{\Phi} \left\{ \sum_{\vec{a} \in \Phi(\lambda)} \bar{N}(\vec{b}|\vec{a}) \right\} = \int_{|\vec{r}|=0}^{R_1} \int_{\varphi=0}^{2\pi} \bar{N}(\vec{b}|\vec{r}) \lambda |\vec{r}| d\varphi d|\vec{r}|, \quad (\text{D.1})$$

where \vec{r} is a vector from $(0, 0)$ to a point within the population circle S_1 and φ is the supplement of the angle between \vec{r} and \vec{b} . We note that $\bar{N}(\vec{b}|\vec{r})$ is obtained by multiplying the point channel response by the emission rate q , integrating over S_0 , and then integrating over all time, i.e.,

$$\begin{aligned} \bar{N}(\vec{b}|\vec{r}) &= \int_{\tau=0}^{\infty} \int_{|\vec{r}_0|=0}^{R_0} \int_{\theta=0}^{2\pi} q C(\vec{d}, \tau) |\vec{r}_0| d\theta d|\vec{r}_0| d\tau, \\ &= \int_{\tau=0}^{\infty} \int_{|\vec{r}_0|=0}^{R_0} \int_{\theta=0}^{2\pi} \frac{q}{(4\pi D\tau)} \exp\left(-\frac{|\vec{d}|^2}{4D\tau} - k\tau\right) |\vec{r}_0| d\theta d|\vec{r}_0| d\tau, \\ &= \int_{\tau=0}^{\infty} \int_{|\vec{r}_0|=0}^{R_0} \int_{\theta=0}^{2\pi} \frac{q}{(4\pi D\tau)} \exp\left(-\frac{|\vec{l}|^2 + |\vec{r}_0|^2 + 2|\vec{l}||\vec{r}_0| \cos \theta}{4D\tau} - k\tau\right) |\vec{r}_0| d\theta d|\vec{r}_0| d\tau, \end{aligned} \quad (\text{D.2})$$

where \vec{l} is a vector from \vec{r} to \vec{b} , i.e., $\vec{l} = \vec{b} - \vec{r}$, \vec{r}_0 is a vector from \vec{b} to a point within the RX circle S_0 , \vec{d} is a vector from \vec{r} to \vec{r}_0 , and θ is the supplement of the angle between \vec{l} and \vec{r}_0 . According to the law of cosines, we obtain $|\vec{l}|^2 = |\vec{b}|^2 + |\vec{r}|^2 + 2|\vec{b}||\vec{r}|\cos\varphi$ and $|\vec{d}|^2 = |\vec{l}|^2 + |\vec{r}_0|^2 + 2|\vec{l}||\vec{r}_0|\cos\theta$. We then apply $|\vec{l}| = \sqrt{|\vec{b}|^2 + |\vec{r}|^2 + 2|\vec{b}||\vec{r}|\cos\varphi}$ to rewrite (D.2) as

$$\begin{aligned} \bar{N}(\vec{b}|\vec{r}) &= \int_{\tau=0}^{\infty} \int_{|\vec{r}_0|=0}^{R_0} \int_{\theta=0}^{2\pi} \frac{q}{(4\pi D\tau)} \exp\left(-\frac{\Upsilon^2(\vec{b})}{4D\tau} - k\tau\right) |\vec{r}_0| d\theta d|\vec{r}_0| d\tau \\ &\stackrel{(a)}{=} \int_{|\vec{r}_0|=0}^{R_0} \int_{\theta=0}^{2\pi} \frac{q}{2D\pi} K_0\left(\sqrt{\frac{k}{D}}\Upsilon(\vec{b})\right) |\vec{r}_0| d\theta d|\vec{r}_0|, \end{aligned} \quad (\text{D.3})$$

where equality (c) is obtained by applying [17, eq. (3.471)]. We finally substitute (D.3) into (D.1) and arrive at (8). This completes the proof.

APPENDIX E

PROOF OF COROLLARY 1, COROLLARY 2, AND COROLLARY 3

We first prove (9). Using UCA, we have

$$\begin{aligned} \bar{N}(\vec{b}|\vec{r}) &\approx \left(\int_{\tau=0}^{\infty} qC(\vec{l}, \tau) d\tau\right) \pi R_0^2 \approx \int_{\tau=0}^{\infty} \frac{q\pi R_0^2}{(4\pi D\tau)} \exp\left(-\frac{|\vec{b}|^2 + |\vec{r}|^2 + 2|\vec{b}||\vec{r}|\cos\varphi}{4D\tau} - k\tau\right) d\tau, \\ &\approx \frac{qR_0^2}{2D} K_0\left(\sqrt{\frac{k}{D}}\Omega(\vec{b})\right). \end{aligned} \quad (\text{E.1})$$

We then substitute (E.1) into (D.1) and obtain (9). (10) can be proven by applying $|\vec{b}| = 0$ to (8). To prove (11), we apply $|\vec{b}| = 0$ to (9) to rewrite (9) as (E.2). By evaluating the final expression of (E.2), we obtain (11).

$$\mathbb{E}_{\Phi}\{\bar{N}_{\text{agg}}(\vec{b}|\lambda)\}\Big|_{|\vec{b}|=0} \approx \int_{|\vec{r}|=0}^{R_1} \int_{\varphi=0}^{2\pi} \frac{qR_0^2}{2D} K_0\left(\sqrt{\frac{k}{D}}|\vec{r}|\right) \lambda|\vec{r}| d\varphi d|\vec{r}| \approx \int_{|\vec{r}|=0}^{R_1} \frac{q\pi R_0^2}{D} K_0\left(\sqrt{\frac{k}{D}}|\vec{r}|\right) \lambda|\vec{r}| d|\vec{r}|. \quad (\text{E.2})$$

APPENDIX F

PROOF OF LEMMA 1

We rewrite (12) as

$$\begin{aligned} \tilde{\text{Pr}}(N_{\text{agg}}^{\dagger}(\vec{x}_i|\lambda) \geq \eta) &\stackrel{(a)}{=} 1 - \mathbb{E}_{\Phi}\left\{\sum_{n=0}^{\eta-1} \frac{1}{n!} \exp\left\{-\bar{N}_{\text{agg}}^{\dagger}(\vec{x}_i|\lambda)\right\} \left(\bar{N}_{\text{agg}}^{\dagger}(\vec{x}_i|\lambda)\right)^n\right\} \\ &\stackrel{(b)}{=} 1 - \sum_{n=0}^{\eta-1} \frac{1}{n!} \mathbb{E}_{\Phi}\left\{\frac{\partial^n \exp\left\{\bar{N}_{\text{agg}}^{\dagger}(\vec{x}_i|\lambda)\rho\right\}}{\partial \rho^n}\right\}\Bigg|_{\rho=-1} \stackrel{(c)}{=} 1 - \sum_{n=0}^{\eta-1} \frac{1}{n!} \frac{\partial^n \mathbb{E}_{\Phi}\left\{\exp\left\{\bar{N}_{\text{agg}}^{\dagger}(\vec{x}_i|\lambda)\rho\right\}\right\}}{\partial \rho^n}\Bigg|_{\rho=-1}, \end{aligned} \quad (\text{F.1})$$

where equality (a) is due to the CDF of Poisson RV $N_{\text{agg}}^\dagger(\vec{x}_i|\lambda)$. Equality (b) is due to exchanging the order of sum and expectation and $\exp\left\{-\overline{N}_{\text{agg}}^\dagger(\vec{x}_i|\lambda)\right\}\left(\overline{N}_{\text{agg}}^\dagger(\vec{x}_i|\lambda)\right)^n = \left.\frac{\partial^n \exp\left\{\overline{N}_{\text{agg}}^\dagger(\vec{x}_i|\lambda)\rho\right\}}{\partial \rho^n}\right|_{\rho=1}$ in [40]. Equality (c) is due to exchanging the order of derivative and expectation. Applying $\mathcal{L}_{\overline{N}_{\text{agg}}^\dagger(\vec{x}_i|\lambda)}(s) = \mathbb{E}_\Phi\left\{\exp\left\{-s\overline{N}_{\text{agg}}^\dagger(\vec{x}_i|\lambda)\right\}\right\}$ to (F.1), we obtain (13).

APPENDIX G

PROOF OF LEMMA 2

We first recall that the bacterium i observes molecules in the environment released from all bacteria (also including the molecules released from itself). Thus, we have

$$\overline{N}_{\text{agg}}^\dagger(\vec{x}_i|\lambda) = \sum_{\vec{x}_j \in \Phi(\lambda)} \overline{N}(\vec{x}_i|\vec{x}_j) = \overline{N}(\vec{x}_i|\vec{x}_i) + \sum_{\vec{x}_j \in \Phi(\lambda)/\vec{x}_i} \overline{N}(\vec{x}_i|\vec{x}_j) = \overline{N}_{\text{self}} + \sum_{\vec{a} \in \Phi(\lambda)} \overline{N}(\vec{x}_i|\vec{a}), \quad (\text{G.1})$$

where $\overline{N}_{\text{self}}$ is given in (6). We consider a new density λ to keep the average number of bacteria the same after the approximation of (G.1). We then apply (G.1) to $\mathcal{L}_{\overline{N}_{\text{agg}}^\dagger(\vec{x}_i|\lambda)}(s)$ to rewrite it as

$$\begin{aligned} \mathcal{L}_{\overline{N}_{\text{agg}}^\dagger(\vec{x}_i|\lambda)}(s) &= \mathbb{E}_\Phi\left\{\exp\left\{-s\left\{\sum_{\vec{a} \in \Phi(\lambda)} \overline{N}(\vec{x}_i|\vec{a}) + \overline{N}_{\text{self}}\right\}\right\}\right\}, \\ &= \exp(-s\overline{N}_{\text{self}}) \mathbb{E}_\Phi\left\{\prod_{\vec{a} \in \Phi(\lambda)} \exp\left\{-s\overline{N}(\vec{x}_i|\vec{a})\right\}\right\}. \end{aligned} \quad (\text{G.2})$$

Using the probability generating functional (PGFL) for the PPP [39, eq. (4.8)], we rewrite (G.2) as (14). This completes the proof.

APPENDIX H

PROOF OF THEOREM 6

Using the definition of MGF [41], the MGF of Z is given by $M_Z(u) = \mathbb{E}\{\exp(uZ)\}$. We substitute $Z = \sum_{\vec{x}_i \in \Phi(\lambda)} B(\vec{x}_i, \Phi)$ into $M_Z(u) = \mathbb{E}\{\exp(uZ)\}$ to rewrite $M_Z(u)$ as

$$M_Z(u) = \mathbb{E}\left\{\exp\left(u \sum_{\vec{x}_i \in \Phi(\lambda)} B(\vec{x}_i, \Phi)\right)\right\} = \mathbb{E}\left\{\prod_{\vec{x}_i \in \Phi(\lambda)} \exp\left(uB(\vec{x}_i, \Phi)\right)\right\}. \quad (\text{H.1})$$

The expectation in (H.1) is averaged over many realizations of randomly-distributed bacteria locations and their binary decisions. Thus, the expectation in (H.1) can be written as first averaging over

the binary decisions of bacteria and then averaging over the spatial point process Φ . By doing so, we rewrite (H.1) as

$$\begin{aligned}
M_Z(u) &= \mathbb{E}_\Phi \left\{ \prod_{\vec{x}_i \in \Phi(\lambda)} \mathbb{E}_B \{ \exp(uB(\vec{x}_i, \Phi)) \} \right\} \\
&\stackrel{(a)}{=} \mathbb{E}_\Phi \left\{ \prod_{\vec{x}_i \in \Phi(\lambda)} \{ \exp(u) \Pr(B(\vec{x}_i, \Phi) = 1) + (1 - \Pr(B(\vec{x}_i, \Phi) = 1)) \} \right\} \\
&= \mathbb{E}_\Phi \left\{ \prod_{\vec{x}_i \in \Phi(\lambda)} \{ 1 + (\exp(u) - 1) \Pr(B(\vec{x}_i, \Phi) = 1) \} \right\}, \tag{H.2}
\end{aligned}$$

where equality (a) is because $B(\vec{x}_i, \Phi)$ is a Bernoulli RV with mean $\Pr(B(\vec{x}_i, \Phi) = 1)$. We recall that the bacterium i is a cooperator, i.e., $B(\vec{x}_i, \Phi) = 1$, if $N_{\text{agg}}^\dagger(\vec{x}_i|\lambda)$ is larger than η . Thus, we derive $\Pr(B(\vec{x}_i, \Phi) = 1)$ as

$$\Pr(B(\vec{x}_i, \Phi) = 1) = \Pr\left(N_{\text{agg}}^\dagger(\vec{x}_i|\lambda) \geq \eta | \bar{N}_{\text{agg}}^\dagger(\vec{x}_i|\lambda)\right), \tag{H.3}$$

where $\Pr\left(N_{\text{agg}}^\dagger(\vec{x}_i|\lambda) \geq \eta | \bar{N}_{\text{agg}}^\dagger(\vec{x}_i|\lambda)\right)$ is the conditional cooperating probability for the bacterium i in a given realization of the spatial random point process Φ . Analogously to Sec. IV-A, we assume that $N_{\text{agg}}^\dagger(\vec{x}_i|\lambda)$ is a Poisson RV and apply $\bar{N}_{\text{agg}}^\dagger(\vec{x}_i|\lambda) = \sum_{\vec{x}_j \in \Phi(\lambda)} \bar{N}(\vec{x}_i|\vec{x}_j)$ to rewrite (H.3) as

$$\begin{aligned}
\Pr(B(\vec{x}_i, \Phi) = 1) &= 1 - \left(\sum_{n=0}^{\eta-1} \frac{1}{n!} \exp\left\{-\bar{N}_{\text{agg}}^\dagger(\vec{x}_i|\lambda)\right\} \left(\bar{N}_{\text{agg}}^\dagger(\vec{x}_i|\lambda)\right)^n \right) \\
&= 1 - \left(\sum_{n=0}^{\eta-1} \frac{1}{n!} \exp\left\{-\sum_{\vec{x}_j \in \Phi(\lambda)} \bar{N}(\vec{x}_i|\vec{x}_j)\right\} \left(\sum_{\vec{x}_j \in \Phi(\lambda)} \bar{N}(\vec{x}_i|\vec{x}_j)\right)^n \right). \tag{H.4}
\end{aligned}$$

We finally substitute (H.4) into (H.2), we obtain (20).

APPENDIX I

PROOF OF THEOREM 7

To obtain (22), we use the expected cooperating probability over the spatial point process Φ to approximate the conditional cooperating probability for a given instantaneous realization of this point process Φ . By doing so, we approximate (H.3) as

$$\Pr(B(\vec{x}_i, \Phi) = 1) \approx \mathbb{E}_\Phi \left\{ \Pr(B(\vec{x}_i, \Phi) = 1) \right\}, \tag{I.1}$$

$$\mathbb{E}_\Phi \left\{ \Pr(B(\vec{x}_i, \Phi) = 1) \right\} = \mathbb{E}_\Phi \left\{ \Pr\left(N_{\text{agg}}^\dagger(\vec{x}_i|\lambda) \geq \eta | \bar{N}_{\text{agg}}^\dagger(\vec{x}_i|\lambda)\right) \right\} = \tilde{\Pr}\left(N_{\text{agg}}^\dagger(\vec{x}_i|\lambda) \geq \eta\right), \tag{I.2}$$

where $\tilde{\Pr}\left(N_{\text{agg}}^\dagger(\vec{x}_i|\lambda) \geq \eta\right)$ is evaluated in Sec. IV. The approximated $\Pr(B(\vec{x}_i, \Phi) = 1)$ in (I.1) only depends on the location \vec{x}_i and does not depend on the position of other bacteria in Φ .

We then substitute (I.1) into (H.2) and obtain the approximated $M_Z(u)$ as

$$M_Z(u) \approx \mathbb{E}_\Phi \left\{ \prod_{\vec{x}_i \in \Phi(\lambda)} \{1 + (\exp(u) - 1) \tilde{\Pr}(N_{\text{agg}}^\dagger(\vec{x}_i|\lambda) \geq \eta)\} \right\}. \quad (\text{I.3})$$

Using PGFL [39, eq. (4.8)] for a PPP, we derive (I.3) as (22). Based on (22), we obtain (23) via $\mathcal{K}_Z(u) = \log \mathbb{E}_\Phi \{\exp(uZ)\}$. This completes the proof.

APPENDIX J

PROOF OF PROPOSITION 2

Recalling $Z = \sum_{\vec{x}_i \in \Phi(\lambda)} B(\vec{x}_i, \Phi)$, we directly write $\mathbb{E}_\Phi\{Z\}$ (instead of using the MGF of Z) as

$$\mathbb{E}_\Phi\{Z\} = \mathbb{E}_\Phi\{\bar{Z}\} = \mathbb{E}_\Phi \left\{ \sum_{\vec{x}_i \in \Phi(\lambda)} \Pr(B(\vec{x}_i, \Phi) = 1) \right\}, \quad (\text{J.1})$$

where \bar{Z} is the mean of Z for a given instantaneous realization of Φ . Applying Campbell-Mecke's theorem of PPPs [39, eq. (8.7)] given by $\mathbb{E}_\Phi \left\{ \sum_{x \in \Phi} h(x, \Phi) \right\} = \lambda \int_{\mathbb{R}^2} \mathbb{E}_\Phi(h(x, \Phi)) dx$ to (J.1), we rewrite (J.1) as

$$\mathbb{E}_\Phi \left\{ \sum_{\vec{x}_i \in \Phi(\lambda)} \Pr(B(\vec{x}_i, \Phi) = 1) \right\} = \int_{|\vec{r}_1|=0}^{R_1} \mathbb{E}_\Phi \{ \Pr(B(\vec{r}_1, \Phi) = 1) \} \lambda 2\pi |\vec{r}_1| d|\vec{r}_1|. \quad (\text{J.2})$$

Applying (H.3) and (12) to (J.2), we arrive at (26), which completes the proof.

APPENDIX K

PROOF OF THEOREM 9

For any node \vec{x}_i , we evaluate $\Pr(B(\vec{x}_{i,n}) = 1)$ as

$$\Pr(B(\vec{x}_{i,n}, \Phi) = 1) = \int_{|\vec{r}_2|=0}^{R_1} \int_{\psi=0}^{2\pi} \Pr(B(\vec{r}_2, \Phi) = 1) \frac{g_n(r(\vec{x}_i))}{2\pi r(\vec{x}_i)} |\vec{r}_2| d|\vec{r}_2| d\psi, \quad (\text{K.1})$$

where \vec{r}_2 is a vector from $(0,0)$ to a point within the population circle S_1 and ψ is the supplement of the angle between \vec{r}_2 and \vec{x}_i , $r(\vec{x}_i)$ is the distance between \vec{r}_2 and \vec{x}_i , i.e., $r(\vec{x}_i) = \sqrt{|\vec{r}_2|^2 + |\vec{x}_i|^2 + 2|\vec{r}_2||\vec{x}_i|\cos\psi}$, and $g_n(r)$ is the probability density function (PDF) of distance r given by $g_n(r) = \frac{2}{\Gamma(n)} (\lambda\pi)^n r^{2n-1} \exp(-\lambda\pi r^2)$ [39, eq. (2.12)]. Applying (K.1) to (30), we rewrite $P(n)$ as

$$P(n) = \mathbb{E}_\Phi \left\{ \sum_{\vec{x}_i \in \Phi(\lambda)} \left\{ \Pr(B(\vec{x}_i, \Phi) = 1) \int_{|\vec{r}_2|=0}^{R_1} \int_{\psi=0}^{2\pi} \Pr(B(\vec{r}_2, \Phi) = 1) \frac{g_n(r(\vec{x}_i))}{2\pi r(\vec{x}_i)} |\vec{r}_2| d|\vec{r}_2| d\psi \right\} \right\}. \quad (\text{K.2})$$

Using $\mathbb{E}_\Phi \left\{ \sum_{x \in \Phi} h(x, \Phi) \right\} = \lambda \int_{\mathbb{R}^2} \mathbb{E}_\Phi(h(x, \Phi)) dx$ and (I.2), we rewrite (K.2) as (31).

APPENDIX L
 NUMERICAL RESULTS FOR REMARK 6

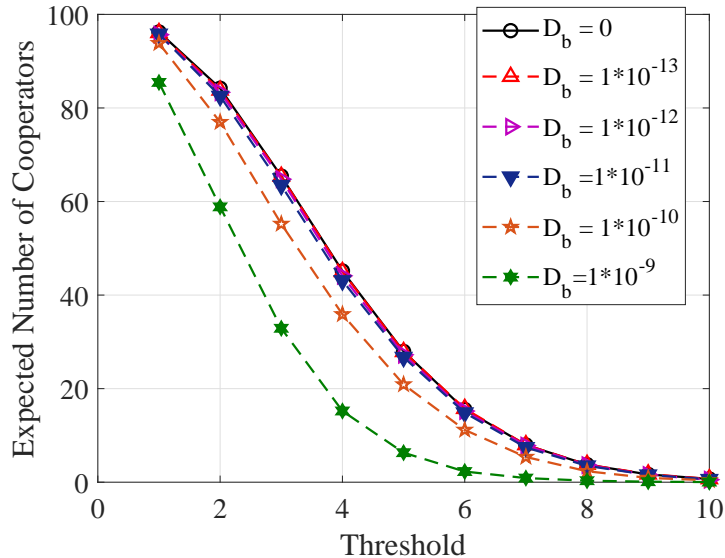


Fig. 12. Expected number of cooperative bacteria versus detection threshold for different diffusion coefficients of mobile bacteria D_b . $R_1 = 50 \mu\text{m}$, expected number of bacteria is 100, and other parameters are the same as those in Section VI.

In Fig. 12, we plot expected number of cooperative bacteria versus detection threshold for different diffusion coefficients of mobile bacteria D_b . We see that the expected number of cooperative bacteria decreases as the diffusion coefficient increases (i.e., bacteria move faster), which meets the Reviewer’s expectation (i.e., the cooperation probability is less). This is because when bacteria move faster, the average distance between bacteria is larger and fewer molecules are observed, which leads to a smaller cooperation probability and fewer cooperators. We also see that in comparison to the non-mobile case (i.e., $D_b = 0$), the impact of increasing D_b on reducing the number of cooperators is not linear. For example, increasing D_b from 0 to $D_b = 10^{-11}$ leads to a negligible drop in the number of cooperators, while increasing D_b from $D_b = 10^{-11}$ to $D_b = 10^{-9}$ leads to 66% drop of the number of cooperators when the threshold at $\eta = 4$. These values may be large for bacteria to diffuse as they are on the order of what we expect for small molecules in water. Though perhaps bacteria can “diffuse” this fast via more active means, e.g., via chemotaxis.

REFERENCES

- [1] Y. Fang, A. Noel, A. W. Eckford, and N. Yang, “Expected density of cooperative bacteria in a 2D quorum sensing based molecular communication system,” in *Proc. IEEE GLOBECOM*, Dec. 2019, pp. 1–7.

- [2] J. Boedicker and K. Neelson, "Microbial communication via quorum sensing," *IEEE Trans. Mol. Bio. Multi-Scale Commun.*, vol. 1, no. 4, pp. 310–320, Dec. 2015.
- [3] T. Czrn and R. F. Hoekstra, "Microbial communication, cooperation and cheating: Quorum sensing drives the evolution of cooperation in bacteria," *PLOS ONE*, vol. 4, no. 8, pp. 1–10, Aug. 2009.
- [4] S. A. West, A. S. Griffin, and A. Gardner, "Social semantics: Altruism, cooperation, mutualism, strong reciprocity and group selection," *J. Evol. Bio.*, vol. 20, no. 2, pp. 415–432, Mar. 2007.
- [5] R. J. Lindsay, B. J. Pawlowska, and I. Gudelj, "When increasing population density can promote the evolution of metabolic cooperation," *The ISME J.*, vol. 12, pp. 849–859, Jan. 2017.
- [6] A. Noel, Y. Fang, N. Yang, D. Makrakis, and A. W. Eckford, "Effect of local population uncertainty on cooperation in bacteria," in *Proc. IEEE ITW*, Nov. 2017, pp. 334–338.
- [7] L. Canzian, K. Zhao, G. C. L. Wong, and M. van der Schaar, "A dynamic network formation model for understanding bacterial self-organization into micro-colonies," *IEEE Trans. Mol. Bio. Multi-Scale Commun.*, vol. 1, no. 1, pp. 76–89, Mar. 2015.
- [8] C. Koca and O. B. Akan, "Anarchy versus cooperation on internet of molecular things," *IEEE Internet Things J.*, vol. 4, no. 5, pp. 1445–1453, Oct. 2017.
- [9] M. M. Vasconcelos, U. Mitra, O. Camara, K. P. Silva, and J. Boedicker, "Bacterial quorum sensing as a networked decision system," in *Proc. IEEE ICC*, May 2018, pp. 1–6.
- [10] N. Michelusi, J. Boedicker, M. Y. El-Naggar, and U. Mitra, "Queuing models for abstracting interactions in bacterial communities," *IEEE J. Select. Areas Commun.*, vol. 34, no. 3, pp. 584–599, Mar. 2016.
- [11] B. D. Unluturk, S. Balasubramaniam, and I. F. Akyildiz, "The impact of social behavior on the attenuation and delay of bacterial nanonetworks," *IEEE Trans. Nanobiosci.*, vol. 15, no. 8, pp. 959–969, Dec. 2016.
- [12] A. Einolghozati, M. Sardari, and F. Fekri, "Design and analysis of wireless communication systems using diffusion-based molecular communication among bacteria," *IEEE Trans. Wireless Commun.*, vol. 12, no. 12, pp. 6096–6105, Dec. 2013.
- [13] F. Baccelli and B. Blaszczyszyn, *Stochastic Geometry and Wireless Networks in Foundations and Trends in Networking*, 2010.
- [14] M. Haenggi, J. G. Andrews, F. Baccelli, O. Dousse, and M. Franceschetti, "Stochastic geometry and random graphs for the analysis and design of wireless networks," *IEEE J. Select. Areas Commun.*, vol. 27, no. 7, pp. 1029–1046, Sep. 2009.
- [15] C. Picioreanu, M. C. M. van Loosdrecht, and J. J. Heijnen, "Two-dimensional model of biofilm detachment caused by internal stress from liquid flow," *Biotechnology and Bioengineering*, vol. 72, no. 2, pp. 205–218, Dec. 2000.
- [16] S. Abadal and I. F. Akyildiz, "Bio-inspired synchronization for nanocommunication networks," in *Proc. IEEE GLOBECOM*, Dec. 2011, pp. 1–5.
- [17] I. S. Gradshteyn and I. M. Ryzhik, *Table of integrals, series, and products*, 7th ed. Amsterdam, Netherlands: Elsevier/Academic Press, 2007.
- [18] M. Haenggi and R. K. Gant, "Interference in large wireless networks," *Foundations and Trends in Networking*, 2009.
- [19] A. Noel, K. C. Cheung, and R. Schober, "A unifying model for external noise sources and isi in diffusive molecular communication," *IEEE J. Select. Areas Commun.*, vol. 32, no. 12, pp. 2330–2343, 2014.
- [20] A. Etemadi, P. Azmi, H. Arjmandi, and N. Mokari, "Compound poisson noise sources in diffusion-based molecular communication," *IEEE Trans. Commun.*, vol. 67, no. 6, pp. 4104–4116, 2019.
- [21] T. Danino, O. Mondragón-Palomino, L. S. Tsimring, and J. Hasty, "A synchronized quorum of genetic clocks," *Nature*, vol. 463, pp. 326–330, Jan. 2010.
- [22] A. Trovato, F. Seno, M. Zanardo, S. Alberghini, A. Tondello, and A. Squartini, "Quorum vs. diffusion sensing: A quantitative analysis of the relevance of absorbing or reflecting boundaries," *FEMS Microbiology Lett.*, vol. 352, no. 2, pp. 198–203, Jan. 2014.
- [23] M. G. Surette and B. L. Bassler, "Quorum sensing in *Escherichia coli* and *Salmonella typhimurium*," *Proc. Nat. Academy Sci.*, vol. 95, no. 12, pp. 7046–7050, Jun. 1998.

- [24] B. Tepekule, A. E. Pusane, H. B. Yilmaz, C. Chae, and T. Tugcu, "ISI mitigation techniques in molecular communication," *IEEE Trans. Mol. Bio. Multi-Scale Commun.*, vol. 1, no. 2, pp. 202–216, June 2015.
- [25] Y. Lin, W. Lin, C. Lee, and P. Yeh, "Asynchronous threshold-based detection for quantity-type-modulated molecular communication systems," *IEEE Trans. Mol. Bio. Multi-Scale Commun.*, vol. 1, no. 1, pp. 37–49, March 2015.
- [26] A. Noel, Y. Fang, N. Yang, D. Makrakis, and A. W. Eckford, "Using game theory for real-time behavioral dynamics in microscopic populations with noisy signaling," pp. 1–10, 2019. [Online]. Available: arXiv:1711.04870
- [27] R. Salahat, E. Salahat, A. Hakam, and T. Assaf, "A simple and efficient approximation to the modified Bessel functions and its applications to Rician fading," in *Proc. IEEE GCC*, Nov 2013, pp. 351–354.
- [28] A. Noel, K. C. Cheung, and R. Schober, "Using dimensional analysis to assess scalability and accuracy in molecular communication," in *Proc. IEEE ICC*, June 2013, pp. 818–823.
- [29] F. Francesco, "Note sur une nouvelle formule de calcul differentiel," *The Quarterly Journal of Pure and Applied Mathematics*, no. 1, pp. 359–360, 1857.
- [30] R. Hogg and A. T. Craig, *Introduction to Mathematical Statistics*, 6th ed. Pearson, 2004.
- [31] L. DeCarlo, "On the meaning and use of kurtosis," *Psychological Methods*, vol. 2, pp. 292–307, 09 1997.
- [32] S. Srinivasa and M. Haenggi, "Modeling interference in finite uniformly random networks," in *WITS 2007*, June 2007, pp. 1–12.
- [33] G. E. Dilanji, J. B. Langebrake, P. D. Leenheer, and S. J. Hagen, "Quorum activation at a distance: spatiotemporal patterns of gene regulation from diffusion of an autoinducer signal." *J. Am. Chem. Soc.*, vol. 134, no. 12, pp. 5618–5626, 2012.
- [34] S. S. Andrews and D. Bray, "Stochastic simulation of chemical reactions with spatial resolution and single molecule detail," *Physical Biology*, vol. 1, no. 3, pp. 135–151, Aug. 2004.
- [35] A. Noel, K. C. Cheung, and R. Schober, "Improving receiver performance of diffusive molecular communication with enzymes," *IEEE Trans. Nanobiosci.*, vol. 13, no. 1, pp. 31–43, Mar. 2014.
- [36] V. Jamali, A. Ahmadzadeh, W. Wicke, A. Noel, and R. Schober, "Channel modeling for diffusive molecular communication—a tutorial review," *Proceedings of the IEEE*, vol. 107, no. 7, pp. 1256–1301, July 2019.
- [37] O. M. Cloak, B. T. Solow, C. E. Briggs, C.-Y. Chen, and P. M. Fratamico, "Quorum sensing and production of autoinducer-2 in campylobacter spp., escherichia coli o157:h7, and salmonella enterica serovar typhimurium in foods," *Applied and Environmental Microbiology*, vol. 68, no. 9, pp. 4666–4671, 2002.
- [38] J. Crank, *The Mathematics of Diffusion*, 2nd ed. Oxford, UK: Oxford University Press, 1975.
- [39] M. Haenggi, *Stochastic Geometry for Wireless Networks*, 1st ed. MA, NY: Cambridge University Press, 2012.
- [40] Y. Deng, A. Noel, W. Guo, A. Nallanathan, and M. ElKashlan, "Analyzing large-scale multiuser molecular communication via 3-D stochastic geometry," *IEEE Trans. Mol. Bio. Multi-Scale Commun.*, vol. 3, no. 2, pp. 118–133, June 2017.
- [41] S. M. Ross, *Introduction to Probability and Statistics for Engineers and Scientists*, 5th ed. New York, NY: Academic Press, 2014.